



UNIVERSITATEA BABEȘ-BOLYAI



Facultatea de Chimie și Inginerie Chimică

Theoretical studies in cluster chemistry – OR - Synthesis – a Ph adjustment of Ph.D.



Student: Adrian M.V. Brânzanic

Advisor: Prof. Radu Silaghi-Dumitrescu

Extended summary of the
Ph.D. thesis

Cluj-Napoca, 2020

Contents of summary

1	Introduction	1
	The four sapiential stages.....	1
	The <i>eide</i>	3
	About this thesis.....	6
2	The elements.....	8
3	Theoretical studies of hydrogen-rich metallaboranes.....	9
	Systems with 5 vertices.....	9
	Systems with 6 vertices.....	11
	Systems with 7 vertices.....	13
	Systems with 8 vertices.....	15
	Computed structures matching the <i>a priori</i> known metallaboranes	17
	Predicted metallaborane structures confirmed <i>a posteriori</i> by experiments	17
	Chapter Conclusions	20
4	Theoretical investigations of the sulfite reductase active site	21
	Pars energetica: The importance of the siroheme modification.....	21
	Pars ballistica: Why does sulfite reductase employ siroheme?	25
	Pars mechanistica: SiR reaction mechanism.....	28
	Chapter Conclusions	29
5	Epilogue.....	31
6	Thesis references	33

Keywords: *metallaboranes, heme, siroheme, sulfite reductase, electron transfer.*

Thesis's table of contents

1	Introduction	10
1.1	The four sapiential stages	11
1.2	The eide	13
1.3	About this thesis	16
1.3.1	Manifesto	16
1.3.2	Structure	16
1.4	Chapter Bibliography	18
2	The elements	19
2.1	Elements of Quantum Mechanics	20
2.2	Elements of Quale Mechanics	30
2.4	Elements of Computational Chemistry	37
2.4.1	Introduction	37
2.4.2	Molecular Mechanics	38
2.4.3	Quantum Chemistry	41
2.4.3.1	The wavefunction	42
2.4.3.2	The Hamiltonian	45
2.4.3.2.1	The Hartree-Fock method and the exchange interaction	45
2.4.3.2.2	Post Hartree-Fock methods	58
2.4.3.2.3	Semiempirical methods	61
2.4.3.2.4	Density functional theory	62
2.4.3.3	Variational vs. perturbational methods	67
2.4.3.4	Non-relativistic vs. relativistic methods	71
2.4.3.5	Standard vs. Periodic	88
2.4.3.6	Vacuum vs. Solvent environment	91
2.4.3.7	Stationary vs. Non-stationary / equilibrium vs. non-equilibrium	99
2.5	Chapter Bibliography	105

3	Theoretical studies of hydrogen-rich metallaboranes	106
3.1	Introduction	107
3.2	The Wade-Mingos rules	110
3.3	Theoretical methods	116
3.4	5 vertices	118
3.4.1	$\text{Cp}_2\text{M}_2\text{B}_3\text{H}_7$ (M = Pd, Pt) systems	120
3.4.2	$\text{Cp}_2\text{M}_2\text{B}_3\text{H}_7$ (M = Rh, Ir) systems	121
3.4.3	$\text{Cp}_2\text{M}_2\text{B}_3\text{H}_7$ (M=Ru,Os) systems	124
3.4.4	$\text{Cp}_2\text{Re}_2\text{B}_3\text{H}_7$ systems	125
3.4.5	$\text{Cp}_2\text{M}_2\text{B}_3\text{H}_7$ (M=Mo,W) systems	128
3.4.6	The single $\text{Cp}_2\text{Ta}_2\text{B}_3\text{H}_7$ structure	130
3.5	6 vertices	131
3.5.1	$\text{Cp}_2\text{Ir}_2\text{B}_4\text{H}_8$ systems	132
3.5.2	$\text{Cp}_2\text{M}_2\text{B}_4\text{H}_8$ (M = Ru, Os) systems	134
3.5.3	$\text{Cp}_2\text{Re}_2\text{B}_4\text{H}_8$ systems	137
3.5.4	$\text{Cp}_2\text{M}_2\text{B}_4\text{H}_8$ (M = Mo, W) systems	139
3.5.5	$\text{Cp}_2\text{Ta}_2\text{B}_4\text{H}_8$ systems	141
3.6	7 vertices	143
3.6.1	$\text{Cp}_2\text{Ir}_2\text{B}_5\text{H}_9$ systems	145
3.6.2	$\text{Cp}_2\text{M}_2\text{B}_5\text{H}_9$ (M = Ru, Os) systems	146
3.6.3	$\text{Cp}_2\text{Re}_2\text{B}_5\text{H}_9$ systems	148
3.6.4	$\text{Cp}_2\text{M}_2\text{B}_5\text{H}_9$ (M=Mo,W) systems	149
3.6.5	$\text{Cp}_2\text{Ta}_2\text{B}_5\text{H}_9$ systems	151
3.7	8 vertices	153
3.7.1	$\text{Cp}_2\text{M}_2\text{B}_6\text{H}_{10}$ (M = Pd, Pt) systems	154
3.7.2	$\text{Cp}_2\text{M}_2\text{B}_6\text{H}_{10}$ (M=Rh,Ir) systems	156
3.7.3	$\text{Cp}_2\text{M}_2\text{B}_6\text{H}_{10}$ (M = Ru, Os) systems	157

3.7.4	Cp ₂ Re ₂ B ₆ H ₁₀ systems	159
3.7.5	Cp ₂ M ₂ B ₆ H ₁₀ (M = Mo, W) systems	160
3.7.6	Cp ₂ Ta ₂ B ₆ H ₁₀ systems	162
3.8	Computed structures matching the a priori known metallaboranes	164
3.9	Predicted metallaborane structures confirmed a posteriori by experiments	164
3.10	Conclusions	167
4	Theoretical investigations of the sulfite reductase active site	168
4.1	Pars energetica: The importance of the siroheme modification	169
4.1.1	Introduction	169
4.1.2	Theoretical methods	172
4.1.2.1	Biological Models	172
4.1.2.2	Heme models of the sulfite reductase active site	173
4.1.2.3	Computational protocols	175
4.1.3	Results	177
4.1.3.1	Benchmarking	177
4.1.3.2	Difference in porphyrin conjugation	184
4.1.3.3	Spin-state energetics of the SiR models	186
4.1.3.4	Redox potentials	187
4.1.3.5	Fe(siro)heme–SCys bond length	188
4.1.3.6	Energy decomposition analysis (EDA)	188
4.1.3.7	Mayer bond order analysis	189
4.1.3.8	Correlation between distance, bond order and bond strength	192
4.1.4	Summary and conclusions	196
4.2	Pars ballistica: Why does sulfite reductase employ siroheme?	198
4.2.1	Introduction	198
4.2.2	Theoretical methods	200
4.2.2.1	SiR active site models	200

4.2.2.2	Electron-transport device models	200
4.2.2.3	Computational protocols	202
4.2.2.3.1	Donor–acceptor treatment	202
4.2.2.3.2	Non-equilibrium Green’s function coupled with DFT (NEGF-DFT).	202
4.2.2.3.2.1	Molecular junction treatment (explicit NEGF-DFT)	202
4.2.2.3.2.2	Electron route analysis (implicit NEGF-DFT)	203
4.2.3	Results	206
4.2.3.1	Intrinsic properties of the cubane cofactor	206
4.2.3.2	SiR active site as a donor–acceptor molecule	206
4.2.3.3	Explicit NEGF-DFT	209
4.2.3.4	Implicit NEGF-DFT	211
4.2.4	Conclusions	215
4.3	Pars mechanistica: SiR reaction mechanism	216
4.3.1	Introduction	216
4.3.2	Theoretical methods	218
4.3.2.1	Models	218
4.3.2.2	Computational protocols	219
4.3.3	Results	220
4.3.3.1	Linkage isomerism in the sulfite adducts	222
4.3.3.2	Linkage isomerism with SO ₂ and SO ₂ H	224
4.3.3.3	Linkage and redox isomerism with SO and SOH	226
4.3.3.4	Redox isomerism within the sulfide adducts	228
4.3.3.5	Crossroads along the SiR reaction mechanism	230
4.3.4	Conclusions	234
4.4	Chapter Conclusions	237
5	Epilogue	238
6	Appendix	241

6.1	Metallaboranes	242
6.1.1	5 vertices	242
6.1.1.1	$\text{Cp}_2\text{M}_2\text{B}_3\text{H}_7$ (M=Pd,Pt) systems	242
6.1.1.2	$\text{Cp}_2\text{M}_2\text{B}_3\text{H}_7$ (M=Rh,Ir) systems	245
6.1.1.3	$\text{Cp}_2\text{M}_2\text{B}_3\text{H}_7$ (M=Ru,Os) systems	248
6.1.1.4	$\text{Cp}_2\text{Re}_2\text{B}_3\text{H}_7$ systems	253
6.1.1.5	$\text{Cp}_2\text{M}_2\text{B}_3\text{H}_7$ (M=Mo,W) systems	257
6.1.1.6	$\text{Cp}_2\text{Ta}_2\text{B}_3\text{H}_7$ systems	264
6.1.2	6 vertices	266
6.1.2.1	$\text{Cp}_2\text{Ir}_2\text{B}_4\text{H}_8$ systems	266
6.1.2.2	$\text{Cp}_2\text{M}_2\text{B}_4\text{H}_8$ (M=Ru,Os) systems	269
6.1.2.3	$\text{Cp}_2\text{Re}_2\text{B}_4\text{H}_8$ systems	276
6.1.2.4	$\text{Cp}_2\text{M}_2\text{B}_4\text{H}_8$ (M=Mo,W) systems	281
6.1.2.5	$\text{Cp}_2\text{Ta}_2\text{B}_4\text{H}_8$ systems	286
6.1.3	7 vertices	289
6.1.3.1	$\text{Cp}_2\text{Ir}_2\text{B}_5\text{H}_9$ systems	289
6.1.3.2	$\text{Cp}_2\text{M}_2\text{B}_5\text{H}_9$ (M=Ru,Os) systems	293
6.1.3.3	$\text{Cp}_2\text{Re}_2\text{B}_5\text{H}_9$ systems	305
6.1.3.4	$\text{Cp}_2\text{M}_2\text{B}_5\text{H}_9$ (M=Mo,W) systems	309
6.1.3.5	$\text{Cp}_2\text{Ta}_2\text{B}_5\text{H}_9$ systems	319
6.1.4	8 vertices	323
6.1.4.1	$\text{Cp}_2\text{M}_2\text{B}_6\text{H}_{10}$ (M=Pd,Pt) systems	323
6.1.4.2	$\text{Cp}_2\text{M}_2\text{B}_6\text{H}_{10}$ (M=Rh,Ir) systems	329
6.1.4.3	$\text{Cp}_2\text{M}_2\text{B}_6\text{H}_{10}$ (M=Ru,Os) systems	339
6.1.4.4	$\text{Cp}_2\text{Re}_2\text{B}_6\text{H}_{10}$ systems	350
6.1.4.5	$\text{Cp}_2\text{M}_2\text{B}_6\text{H}_{10}$ (M=Mo,W) systems	356
6.1.4.6	$\text{Cp}_2\text{Ta}_2\text{B}_6\text{H}_{10}$ systems	363

6.2	Molecular orbital analysis of the high-spin ferric substrate-free models of the Sulfite reductase active site.	368
6.2.1	Heme, siroheme and cubane frontier orbitals	368
6.2.1.1	Cubane: vacuum vs. solvated MOs	368
6.2.1.2	Heme: vacuum vs. solvated MOs	370
6.2.1.3	Siroheme: vacuum vs. solvated MOs	372
6.2.1.4	Heme vs. siroheme	374
6.2.1.5	SiR active site as an electronic transport device	375
6.2.1.6	Conclusions	375
6.2.2	(Siro)heme-Cubane MO analysis	376
6.2.2.1	Heme-Cubane systems	376
6.2.2.1.1	Ferromagnetic coupled	376
6.2.2.1.1.1	Solvation influence on the vertical MOs	376
6.2.2.1.1.2	Solvation influence on the relaxed MOs	378
6.2.2.1.1.3	Relaxation effects	380
6.2.2.1.2	Antiferromagnetic coupled	382
6.2.2.1.2.1	Solvation influence on the vertical MOs	382
6.2.2.1.2.2	Solvation influence on the relaxed MOs	384
6.2.2.1.2.3	Relaxation effects	386
6.2.2.1.3	Ferromagnetic vs. Antiferromagnetic coupled systems	387
6.2.2.1.4	Conclusions	388
6.2.2.2	Siroheme-Cubane systems	388
6.2.2.2.1	Ferromagnetic coupled	388
6.2.2.2.1.1	Solvation influence on the vertical MOs	388
6.2.2.2.1.2	Solvation influence on the relaxed MOs	390
6.2.2.2.1.3	Relaxation effects	392
6.2.2.2.2	Antiferromagnetic coupled	394
6.2.2.2.2.1	Solvation influence on the vertical MOs	394

6.2.2.2.2	Solvation influence on the relaxed MOs	396
6.2.2.2.3	Relaxation effects	398
6.2.2.3	Ferromagnetic vs. Antiferromagnetic coupled systems	400
6.2.2.4	Conclusions	400
6.2.3	Heme vs. Siroheme in Cubane connected models	400
6.2.3.1	Conclusions	401
6.2.4	General conclusions	402
6.3	Sulfite Reductase	403
6.3.1	Correlation of bond parameters in two-parameters plots	403
6.3.2	Electron conductance in various conformers of SiR active site models	407
6.3.3	Bond distances within substrate-including models	414
6.3.4	Mulliken charge and spin analysis of the SiR intermediates	422
6.3.5	SiR reaction mechanism in vacuum	434
7	References	437

1 Introduction

The four sapiential stages

Knowledge can be revealed in different forms - and depending on the sharpness of the thought employed in order to open the abyss of truth, knowledge can be perceived at various levels of depth. According to Plato, there are four stages at which this perception of knowledge can occur (cf. Figure 1). The shallowest of them is termed εἰκασία (eikasias), representing a state which can be perceived only through images and reflections. The term itself derives from the word εἰκών (eikon), which can be translated to *image, face* or *reflection* (the same word represents the etymological root of the modern English word “icon”). As a first step involving the act of perceiving knowledge, it deals with images and their generation. The rather superficial character of this step is best emphasized in Plato’s words when he states that “the visible Universe is an εἰκών of the intelligible one, which comprise the εἶδη (eide = ideas)”, and that “time is an image of eternity”. The second step deals with the sensorial perception of the image and it is associated with the view developed from this process. This stage of perceiving is referred to as πίστις (pistis), a term which can be translated to *belief, faith, conviction* (the etymology of the word “piety” can be traced to the Latin equivalent of πίστις, *pietas*). These two steps differ from the next two the same way believing differs from comprehending*. Consequently, the third step represents understanding and is termed δῖανοία (dianoia). It also refers to *discursive thinking* and, in general, represents the type of knowledge that can be achieved with the help of sciences. Lastly, the fourth step is ἐπιστήμη (episteme), which represents the true nature of things. This type of knowledge is in opposition to that of δόξα (doxa), which represents *opinions*, and, furthermore, Plato distinguishes ἐπιστήμη from πρακτική (praktike = the science of action) and ποιητική (poietike = the productive science, art, poetry) as being of a pure theoretical nature. He puts the latter two terms at the same level with δῖανοία, while he places the first one, δόξα, between the act of knowing the true things, i.e. ἐπιστήμη, and ignorance, to which he refers the act of knowing about untrue things. Thus, the act of achieving an epistemic type of knowledge implies mining through the previous three levels of perception. Although at the dianoic level of knowledge a three-fold degeneracy occurs, Plato’s reasoning

* Heisenberg, p.32 Cf. section 1.4 of thesis.

emphasizes the need of passing through δίανοια in order to reach επιστήμη, avoiding, thus, the other two, πρακτική and ποιητική. In other words, a symmetry breaking is required in order to remove the dianoic degeneracy such that the epistemic level of knowledge can be achieved, a symmetry breaking that quite resembles the Jahn-Teller effect of fame in modern physical chemistry. If in the latter (Jahn-Teller) case the geometry of a molecule is distorted along one of its symmetry axis such that a more energetically favorable state is achieved, in the former, the 3rd level of knowledge is distorted along the “δίανοια axis” such that a deeper kind of knowledge (i.e. επιστήμη) can be achieved.

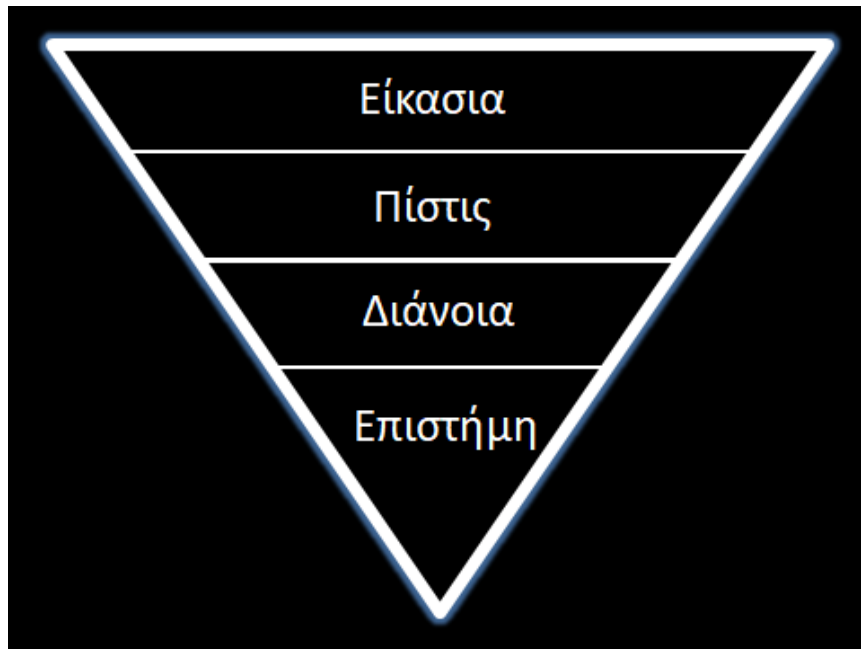


Figure 1. The four stages of the perception of knowledge cf. Plato

The subtle difference between δίανοια and επιστήμη is exemplified in an enlightening manner by Werner Heisenberg in his *“Philosophical Problems of Quantum Physics, p.32”*, where he notes: *“Consider a man, whom we believe we know well, suddenly committing some misdeed which is at first quite incomprehensible. Those who know all the details of the case can then explain the reasons for his action. Thus we are in a position to deal with all the arguments, one after the other, and eventually, after a thorough investigation of these arguments we may understand the wrong he committed. This understanding corresponds to δίανοια. Or*

alternatively we may suddenly realize that this man had to act as he did. This sort of recognition can be described Plato's επιστήμη.” Interestingly by the manner in which the outcome is revealed, the *sudden* epistemic recognition of the truth, which Heisenberg details in his example, resembles the *spontaneous* breaking of symmetry that implies the Jahn-Teller effect. Thus, in a ludic fashion, it can be asserted that the epistemic Jahn-Teller metaphor discussed above shares soil with Heisenberg’s philosophic view. Regarding the role of modern science, Heisenberg stresses that the physical explanation of Nature is a discussion aimed to distinguish *διάνοια* from *επιστήμη*. Regardless if the latter stage is achieved or not, it emphasizes the exclusion of the first two steps of knowledge from the domain in which scientific reasoning should manifest itself.

The *eide*

Returning to the deepest level of perception of things, Plato believes that in order to reach the epistemic level of knowledge, the true nature of things needs to be known. In his view, the *είδη* (*eide*) constitutes the true nature of things that, like in the above-mentioned example regarding the intelligible Universe, are hindered behind appearance. The concept of *είδη*, of the indivisible and eternal entities that lay within the kernel of things, was developed in contrast with the pre-Socratic philosophy which, bearing Heraclitus as exponent, viewed change and fluctuation as the essence of Nature (cf. the famous Heraclitian aphorism *Πάντα ῥεῖ* = Everything flows). Consequently in this line of thought, as everything changes there is no true nature of things, the only constant in Nature being change itself. This fluctuation restricts the achievement of the epistemic level of knowledge and constrains the view of the world within the borders of illusion and temporal truths that are susceptible to fade as time prolongs. In this framework, the highest act of knowing is represented by a *πίστις* → *διάνοια* transition. Plato rejected this framework as the fundamental view of the world and concluded that, in order to achieve the true form of knowledge (i.e. *επιστήμη*), the core of reality should not be subject to change. Interestingly, he refutes the somehow similar atomistic views of Democritus for being materialistic and in a suggestive metaphor he compares its followers to the Titans, while the Olympians are represented by the seekers of *επιστήμη* by means of transcending to a suprasensible picture of reality through the use of the *είδη*. Indeed a godly clash that dislocated the highest act of knowing from a *πίστις* → *διάνοια* transition to a *διάνοια* → *επιστήμη* transition...

The είδη represent the essence of things, the *ideas* that are the fundament of every object. They are of suprasensible nature, meaning that they cannot be grasped through sensorial means. Nevertheless, they can be reached through various rational processes, such as recollection (ανάμνησις) and different forms of dialectics (διαλεκτική). For instance, one of the first dialectical processes consisted in a regression from a hypothesis towards an unhypothesized principle, αρχή. Later, the dialectical process involved a collection/reunion (συναγωγή) followed by a primer division (διαίρεσις) which continues via a second, specific division (διαφορά) downwards the ultimate, indivisible είδος. Examples of eide are found in each class of things such as mathematics, in natural and artificial objects, in relations or even ethics, beauty, goodness. Some of the είδη play a more important role. For instance, for Plato the greatest kinds of είδη are the *Being*, the *Same*, the *Different*, the *Movement* and the *Rest*. By their nature, the είδη are transcendent and form the class of objects by which epistemic knowledge can be revealed. Their collection forms the τόπος νοητός, the intelligible place, are represented as the first concentric circle in Figure 2:

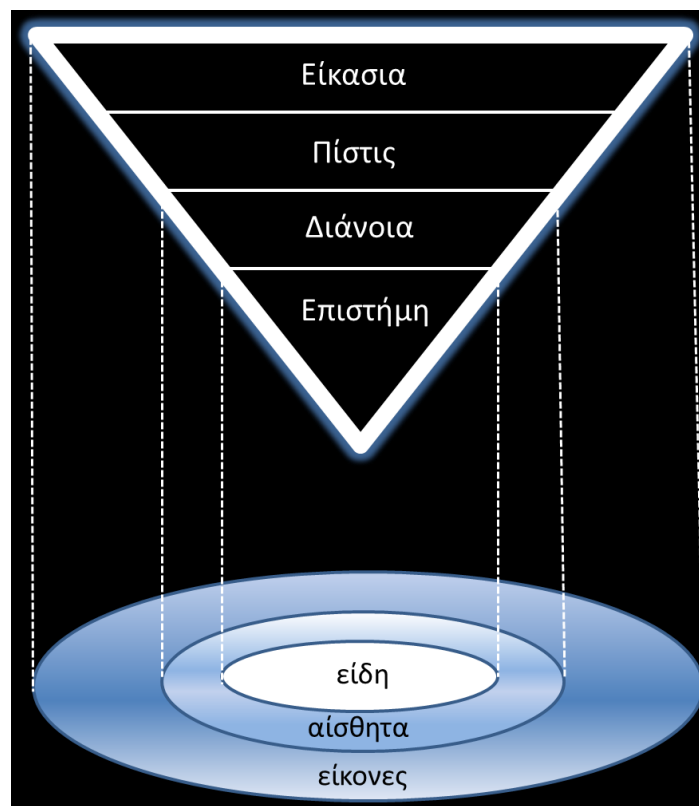


Figure 2. The classes of objects characteristic for different types of knowledge and their corresponding topos: τόπος νοητός in white ; κόσμος and its illusory extension in blue.

Αἴσθησις (aisthesis) represents the sensible nature of things and the objects by which it can be perceived are referred to as *αἴσθητα* (aistheta). They are the source of sensation which, in itself, was regarded as the transition of a sensible entity from its potency (*δύναμις*) to its act (*ἐνέργεια*). Thus, the sensibles, *αἴσθητα*, are objects that are capable of being perceived. They cannot lead to an epistemic level of knowledge but are limited to a dianoic level of knowledge (cf. Figure 2) and therefore can only express opinions. They can still, however, retrieve a deeper level of knowledge than the *εἰκόνες* (eikones) which represent the images, reflections and shadows of things that are therefore restricted to *εἰκασία* and *πίστις* levels of truth. The topos of the sensibles (second concentric circle in Figure 2) bears a name that, through its modern meaning, also emphasizes the alteration that the ancient Greek concepts suffered through the ages: *κόσμος* (cosmos).

The transition from *εἶδος* to *αἴσθησις* is achieved through the intermediate class of the *μέταξά* (metaxy) which, like the eide, are also eternal. The process itself was referred to as *μέθεξις* (methexis) which means *participation*. The difference between the eide and metaxy consists in the plurality nature which the later adopt. Such metaxy objects are represented by the objects of mathematics and geometry. For instance, the ideal numbers (*αριθμοὶ εἰδητικῆ*) are of such character and can modulate the transition between the world of the suprasensible and material world. In some aspects, this picture is not that different from our today's scientific method, which starts from empirical investigations of material objects and then bathes in mathematics in order to build models that can offer prediction. At this stage, more often than not, the similarity ends. The process is no longer descended towards the eide, but rather, in a boomerang manner, is redirected back towards the material world. Perhaps this is one of the crucial differences between us and the Elders. Often enough we restrain our mathematical endeavors to the practical aspects of reality and to its predictability. Blinded by the tempting shine of practical predictions, we ignore the underlying mysteries of the suprasensible world; we too often *shut up and calculate*.

About this thesis

“Lessing, the most honest of theoretical men, dared to state openly that searching for the truth meant more to him than truth itself; thereby the fundamental secret of science is revealed, much to the astonishment, indeed annoyance, of the scientifically minded. Admittedly, alongside this isolated recognition (which represents an excess of honesty, if not of arrogance), one also finds a profound delusion which first appeared in the person of Socrates, namely the imperturbable belief that thought, as it follows the thread of causality, reaches down into the deepest abysses of being, and that it is capable, not simply of understanding existence, but even of correcting it. This sublime metaphysical illusion is an instinct which belongs inseparably to science, and leads it to its limits time after time, at which point it must transform itself into art; which is actually, given this mechanism, what it has been aiming at all along.”[†]

“The regions of science lie far asunder. Their ways of handling their subject matters are fundamentally different. This disintegrated multiplicity of disciplines is still meaningfully maintained today only through the technical organization of universities and faculties and through the practical aims of the disciplines. Yet the rootedness of the sciences in their essential ground has atrophied. In all its areas, science today is a technical, practical matter of gaining information and communicating it. No awakening of the spirit at all can proceed from it as science. Science itself needs such an awakening.”[‡]

This thesis represents the zeroth order term of an attempt towards such an awakening. It can be regarded as a diastole-systole ontological breathing effort. Within the diastole step (left side of Figure 3) a transcendent dive is done into the matter of things by which, in the systole step (right side of Figure 3), a transcendental extraction of available truth is presented as means to justify the original contribution to Science that this PhD offers.

[†] Nietzsche, p. 73 (English). Cf. section 1.4 of thesis.

[‡] Heidegger, *Introduction to Metaphysics*, p. 51 (English). Cf. section 1.4 of thesis.

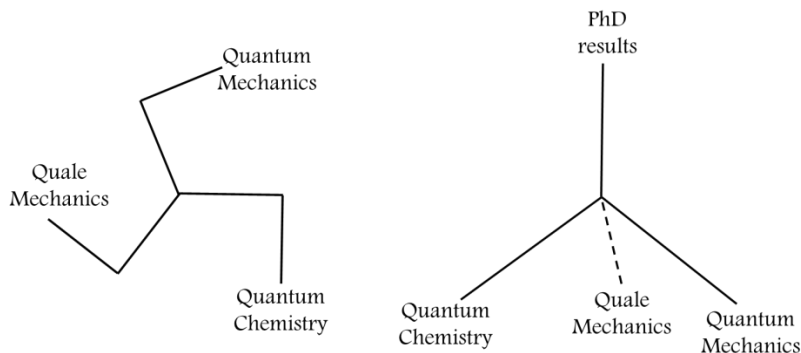


Figure 3. Scheme of current PhD thesis ontological breath.

The present Ph.D. thesis may be argued to entail an *Apollonian-Dionysian* duality. An *Apollonian* character pertains to the majority of the text (metallaboranes, the majority of the study on sulfite reductase), while the philosophical discussions, encountered mainly in the first two chapters of this thesis and in its epilogue, are of *Dionysian* character. The result of the achieved *Apollonian-Dionysian fusion* is best emphasized in the subchapter *Pars ballistica: Why does sulfite reductase employ siroheme?* subchapter which, by revealing the reason behind sulfite reductase's choice for the siroheme, may be viewed as the apex of this thesis in the terms illustrated in Figure 1. In terms of the levels of truth that were surpassed, the question *why does sulfite reductase employ siroheme?* has reached its level where, with regards to the available truth remaining to be unveiled by this question (i.e. none), an epistemic character may be asserted. The *Dionysian* emerges as a thesis which is soon-after complemented by an *Apollonian* antithesis. For instance, in chapter 4.2, the role of siroheme within the sulfite reductase enzyme was first envisioned (i.e a *Dionysian* way) in the thesis that siroheme enhances the enzyme's electron transfer ability; its antithesis would imply that siroheme inhibits those processes. In *Apollonian* manner, the electron transfer ability of sulfite reductase was computed - showing that the reason behind the enzyme's choice for siroheme is an interplay of both thesis and antithesis, as some electron transfer routes were found to be inhibited while others promoted. Thus, a unification of a thesis and its antithesis was achieved which, technically stated, represents a *synthesis*. The title of this dissertation emphasizes this development. Furthermore, it alludes to a need to resurrect the philosophical part of the scientific endeavor and states that such a resurrection is done within its pages. The *Ph* in *Ph.D.* is thus adjusted. We express this by the

metaphorical use of the chemical concept of pH such that the title of this dissertation embodies the “acidity” of the problematic use of Philosophy in Science.

2 The elements

The ongoing chapter develops the constituting elements mentioned on the left side of Figure 3. It starts with a historical presentation of the early development of *Quantum Mechanics* and discusses its comprising axiomatic system. It continues with an original proposal of viewing the quantum phenomena with the aid of metaphysics and coins this new domain of knowledge as *Quale Mechanics*. Presented here in its infancy, parallels between the fundamentals of metaphysics and *Quantum Mechanics* are therefore discussed (i.e. Figure 4). *Quantum Chemistry*, as embedded in *Computational Chemistry*, is presented thereafter by focusing on its pillars.

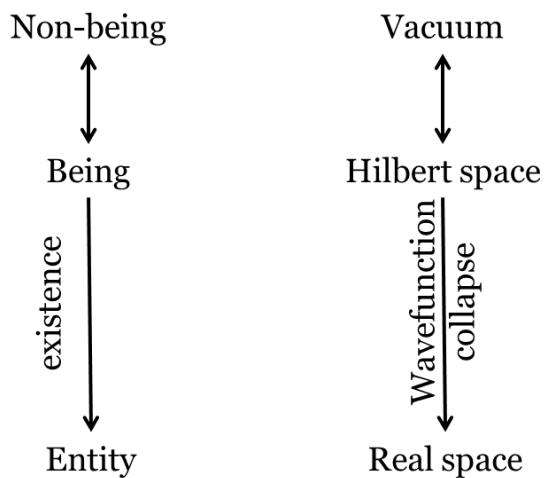


Figure 4. Parallel between Metaphysics (left) and Quantum Mechanics (right).

3 Theoretical studies of hydrogen-rich metallaboranes

Systems with 5 vertices

Historically, the pentaborane represented a high research interest due to its possible military application. After Stone had synthesized and characterized⁷ the structure of the B₅ containing molecule in the early 1930's, it became clear that the pentaborane also contains an extra amount of H atoms within its molecular structure. Similarly to the diborane, the 3c-2e B-H-B bonding scheme was adopted by the pentaborane. However, in the latter case, 4 extra bridging H atoms were harbored on the open square face of the central B₅H₅ square pyramidal framework (cf. left side of Figure 5). This led to a general B₅H₉ nido molecular formula that was also referred to as the *pentaborane-9* molecule. Besides the nido pentaborane, there was another pentaborane species found in lesser amount in the reaction mixture. This species contained 6 extra H atoms and thus had a B₅H₁₁ stoichiometry. This *pentaborane-11*, as it was also referred to, possessed the structure of a square pyramid that had one of its basal edges removed. This led the cluster to become even more opened and now the 6 extra H atoms were divided in 3 bridging atoms and 3 terminal atoms. The overall arachno structure is depicted on the right side of Figure 5. Both molecules became of military interest because of their high amount of stored H, which made plausible candidates as fuels for hydrogen-burning missiles. Because of their lower molecular mass, they also possessed higher heats of combustion than the equivalent hydrocarbons. However, the exhaust substances were toxic and, together with the low stability of these molecules, led to the abandonment of their use as rocket fuels. Nevertheless, by the time of this abandonment, tons of pentaborane had already been obtained.

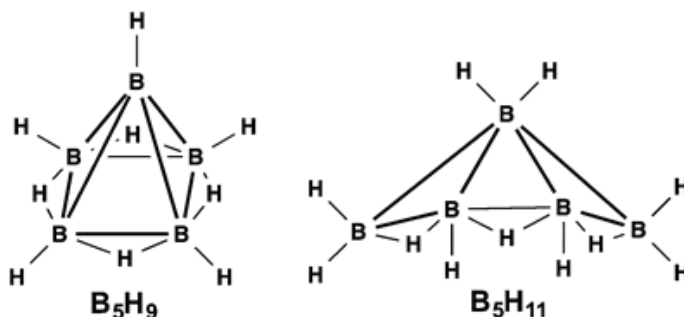


Figure 5. Structures of the two known pentaboranes B₅H₉ and B₅H₁₁.

The structural relationship between the 5-vertices polyhedra is shown in Figure 6. The most spherical 5-vertices deltahedron is represented by the trigonal bipyramid (cf. left side of Figure 6) and it is adopted by the 12 skeletal electron containing $C_2B_3H_5$ molecule.⁴³ The addition of two extra skeletal electrons can lead to the formation of two possible nido geometries. By removing an equatorial-axial edge, the edge-bridged tetrahedron can be obtained (cf. middle-bottom of Figure 6). Removal of an equatorial-equatorial edge followed by a rearrangement of the initial apical vertices can lead to the formation a tetragonal pyramid (cf. middle-top of Figure 6) such as that adopted by the pentaborane-9 molecule. The addition of 2 extra skeletal electrons leads to further removal of a basal-basal edge and to the formation of the open arachno structure such as that of the pentaborane 11 molecule (cf. right side of Figure 6).

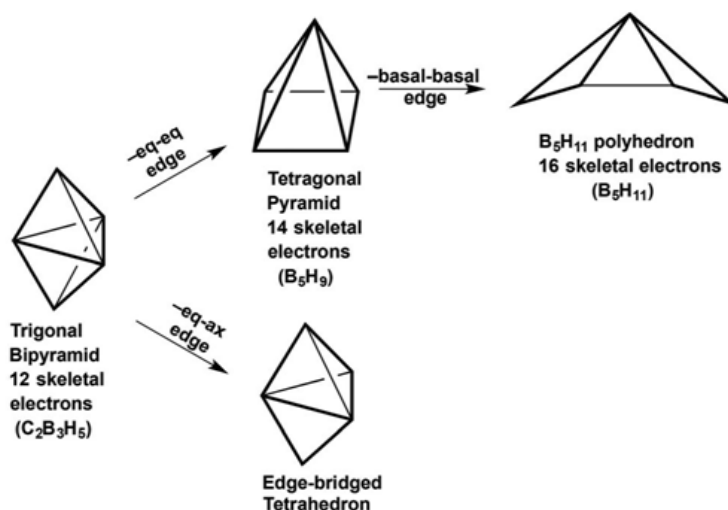


Figure 6. The relationship between the five-vertex polyhedra and the number of skeletal electrons.

The planar pentagon and the tetragonal pyramid were the initial geometries (cf. Figure 7) from which the structures subjected to geometry optimization computations were constructed. The CpM vertices were substituted in all possible ways and the extra four hydrogen atoms were then incorporated as edge-capping atoms on the edges of the tetragonal/pentagonal open face or on the metal–metal edge. This led to 35 different starting geometries to be optimized for each metal family.

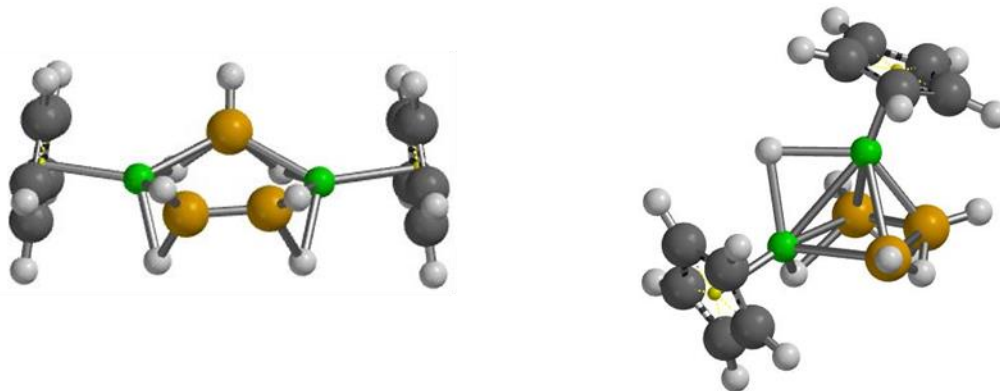


Figure 7. Initial geometries of the $\text{Cp}_2\text{M}_2\text{B}_3\text{H}_7$ ($\text{M} = \text{Pd}, \text{Pt}$) structures and the number of their isomers. Left: the pentagon (32 isomers). Right: the tetragonal pyramid (3 isomers).

Systems with 6 vertices

The process of generating an n -vertex nido polyhedron by the removal of a boron vertex from an $(n + 1)$ vertices deltahedron can be applied not only to the most spherical closo deltahedra, but also to the $(n + 1)$ vertices isocloso and oblatocloso deltahedra. Figure 8 illustrates such processes of vertex removal from seven-vertex deltahedra to give various versions of open six- vertex polyhedra. Thus, the pentagonal bipyramid is the most spherical seven-vertex deltahedron. Removal of a degree 5 vertex from the pentagonal bipyramid gives the pentagonal pyramid. Removal of a degree 4 vertex from the capped octahedron gives a tetragonal prism capped on a triangular face. The closest seven-vertex deltahedron to an oblatocloso deltahedron is a squashed pentagonal bipyramid with the antipodal degree 5 vertices for the metal atoms. Removal of a degree 4 vertex from such a deltahedron generates a bicapped tetrahedron if the original pentagonal bipyramid is squashed enough to have the axial metal atoms within bonding distance.

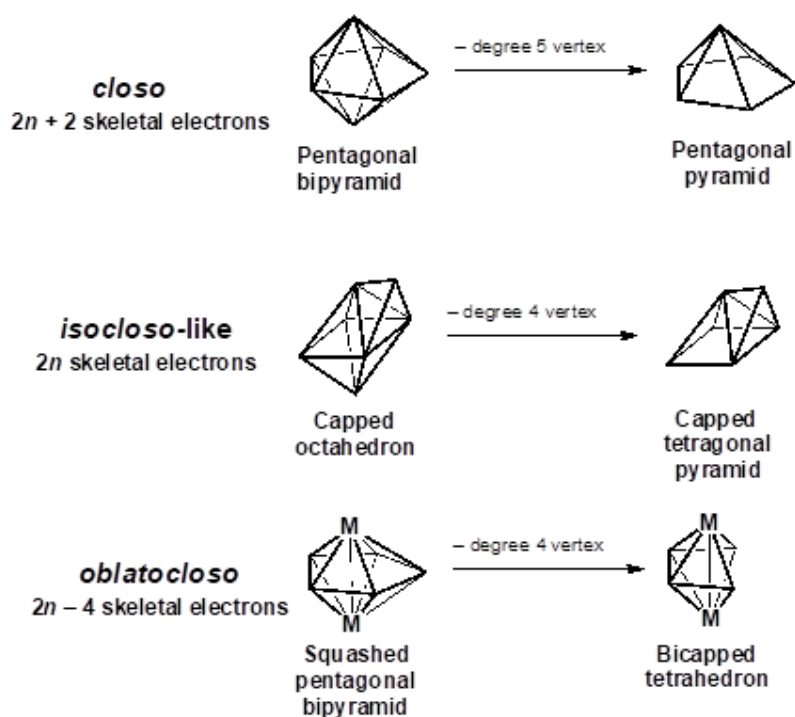


Figure 8. Removal of a vertex in various ways from seven-vertex deltahedra analogous to *closo*, *isocloso*, and *oblatocloso* deltahedra.

The initial $\text{Cp}_2\text{M}_2\text{B}_4\text{H}_8$ structures were constructed by the systematic substitution of the two metal atoms on the vertices of the polyhedra shown in Figure 9. The extra four hydrogen atoms are considered as edge-capping atoms on the edges of the tetragonal/ pentagonal open face or on the metal–metal edge. This leads to 45 different starting geometries to be optimized for each metal system.

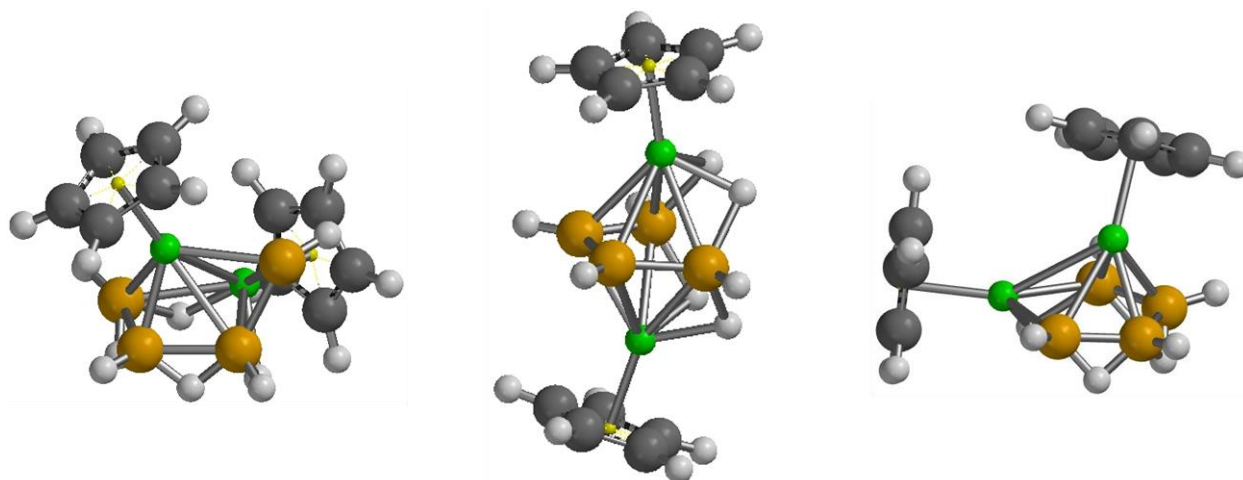


Figure 9. Initial geometries of the $\text{Cp}_2\text{M}_2\text{B}_4\text{H}_8$ structures and the number of their isomers. Left: the capped tetragonal pyramid (16 structures). Middle: the 1 equatorial vertex depleted pentagonal bipyramid (7 isomers) Right: the pentagonal pyramid (22 isomers).

Systems with 7 vertices

The eight-vertex deltahedra that can be used to generate suitable seven-vertex polyhedra for the hydrogen-rich systems by vertex removal include the bisdisphenoid and the hexagonal bipyramid (cf. Figure 10).

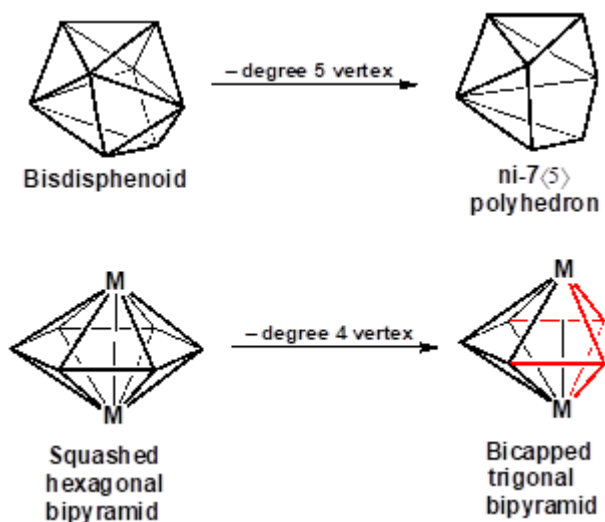


Figure 10. Generation of seven-vertex polyhedra for the hydrogen-rich $\text{Cp}_2\text{M}_2\text{B}_5\text{H}_9$ structures by vertex removal from an eight-vertex deltahedron. The capping vertices and associated edges in the bicapped trigonal bipyramid are shown in red for clarity. Note that the equatorial vertices of

the underlying M_2B_3 trigonal bipyramid form an M_2B triangle including the M-M interaction that was an internal bond in the original squashed hexagonal bipyramid.

Removal of a degree 5 vertex from the bisdisphenoid gives a polyhedron having three degree 3 vertices, three degree 4 vertices, one degree 5 vertex, and a pentagonal open face (cf. top of Figure 10). This polyhedron does not have an obvious name; it will be designated here as ni-7⟨5⟩ using the nomenclature of Williams⁵³ to designate a seven-vertex nido (ni) polyhedron with a pentagonal open face (⟨5⟩). The hexagonal bipyramidal structure from which the polyhedron for some of the $Cp_2M_2B_5H_9$ structures is derived has the metal atoms at the two antipodal degree 6 vertices and is squashed to give an oblate deltahedron with the antipodal metal atoms within bonding distance. Removal of a degree 4 equatorial vertex from a squashed hexagonal bipyramid brings the internal metal-metal bond to the polyhedral surface (cf. bottom of Figure 10). Therefore, the resulting seven-vertex polyhedron does not have an open face but instead remains a deltahedron with all triangular faces. This deltahedron is a bicapped trigonal bipyramid with BH groups capping both M_2B triangular faces of the underlying M_2B_3 trigonal bipyramid.

The initial $Cp_2M_2B_5H_9$ structures were constructed by systematic substitution of two metal atoms in the ni-7⟨5⟩ polyhedron and the bicapped trigonal bipyramid as well as three other seven-vertex polyhedra obtained by vertex removal from the capped pentagonal bipyramid and the bicapped octahedron (cf. Figure 11). The extra four hydrogen atoms are considered as edge-capping atoms on the edges of the tetragonal/ pentagonal open face or on the metal-metal edge. This leads to 81 different starting geometries to be optimized for each metal system.

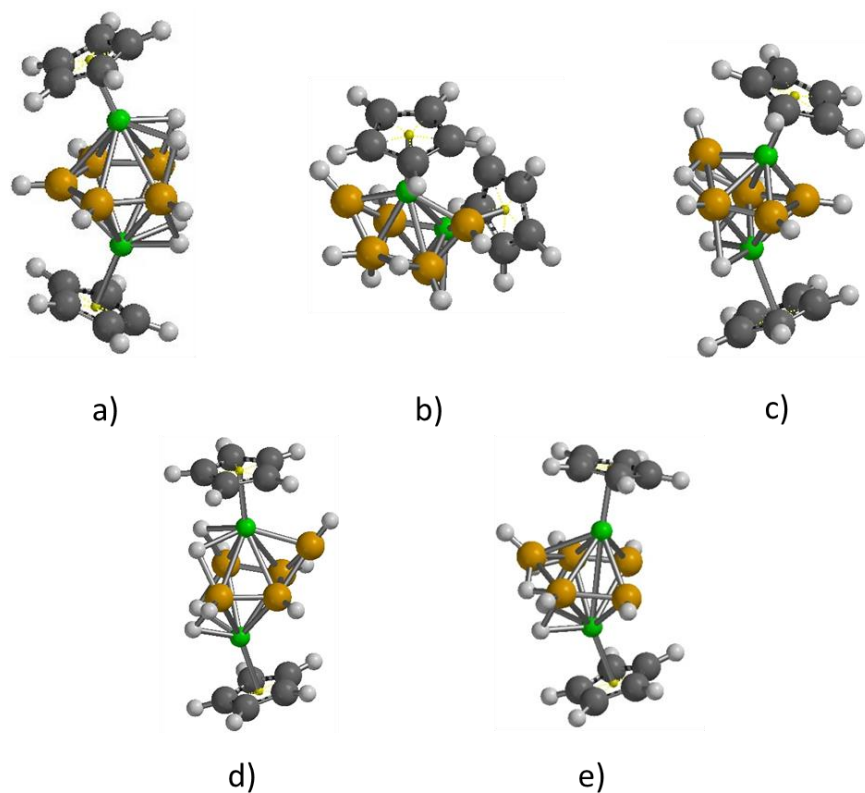


Figure 11. Initial geometries of the $\text{Cp}_2\text{M}_2\text{B}_5\text{H}_9$ structures and the number of their isomers. a) the 1-vertex depleted 8 vertices hexagonal bipyramid (10 structures). b) the 1-vertex depleted 8 vertices dicapped octahedron (8 isomers). c) the 1-vertex depleted 8 vertices bisdisphenoid (12 isomers). d) the 1-vertex depleted 8 capped pentagonal bipyramid (21 isomers). e) the 1-vertex depleted 8 vertices bicapped octahedron (C_s symmetry) (14 isomers).

Systems with 8 vertices

The initial $\text{Cp}_2\text{M}_2\text{B}_6\text{H}_{10}$ structures were constructed by systematic substitution of the two metal atoms on the vertices of the ni-8<5> polyhedron and the B_8H_{12} framework (cf. Figure 12) as well as into three other eight-vertex polyhedra obtained by vertex removal from the capped pentagonal bipyramid and the bicapped octahedron (cf. Figure 13). The extra four hydrogen atoms are considered as edge-capping atoms on the edges of the open face or on the metal-metal edge. This leads to 187 different starting geometries to be optimized for each metal.

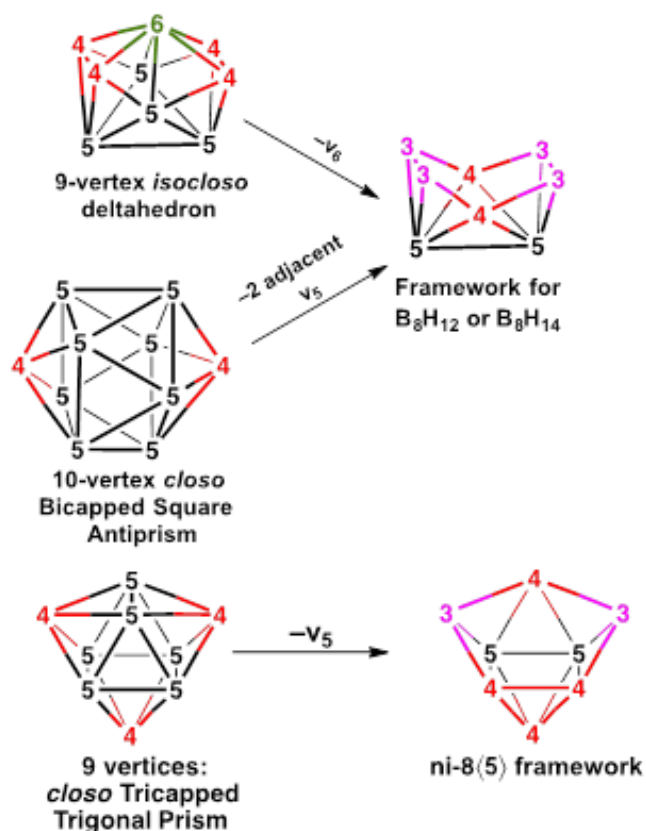


Figure 12. (a) Generation of the 8-vertex framework for either B_8H_{12} or B_8H_{14} by removal of the degree 6 vertex from the *isocloso* 9-vertex deltahedron or by removal of two adjacent degree 5 vertices from the *closo* 10-vertex deltahedron, namely the bicapped square antiprism; (b) Generation of the ni-8(5) framework by removal of a degree 5 vertex from the *closo* 9-vertex deltahedron, namely the tricapped trigonal prism.

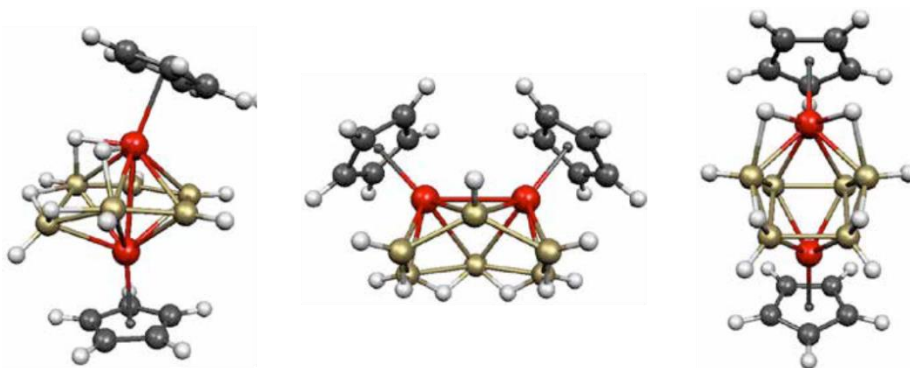


Figure 13. Initial geometries of the $Cp_2M_2B_6H_{10}$ structures and the number of their isomers. Left: the 1-vertex depleted 9 vertices *oblatocloso* (11 structures). Middle: the 1-vertex depleted 9 vertices *isocloso* (77 isomers) Right: the 1-vertex depleted 9 vertices *closo* (99 isomers).

Computed structures matching the *a priori* known metallaboranes

Throughout this chapter there were 34 predicted hydrogen-rich metallaborane structures: 10 structures for the 5-vertices systems, 7 structures for the 6-vertices systems, 7 structures for the 7-vertices systems and 10 structures for the 8-vertices systems. By the time of our computed predictions, there were 8 known experimental structures. Table 1 collects these previously known metallaborane structures alongside their corresponding ground states revealed by the computations within this chapter. The adopted geometries and metal-metal bond lengths are provided for both experimental and theoretical characterized structures. Furthermore, the references leading to the papers in which both experimental and theoretical determined structures were published is also provided. All the computed ground states match the experimentally known hydrogen-rich dimetallaboranes.

Table 1. *A priori* known structures and their corresponding computed ground states.

#	V	A priori experimentally determined structure				Computationally determined structure			
		Metallaborane	Geometry	M-M (Å)	Ref.	Geometry	M-M (Å)	Ref.	
1	5	$\text{Cp}^*_2\text{Rh}_2\text{B}_3\text{H}_7$	Tetragonal pyramid	2.689	45	Tetragonal pyramid	2.689	59	
2		$\text{Cp}^*_2\text{Ir}_2\text{B}_4\text{H}_8$	Pentagonal pyramid	2.738	48,49	Pentagonal pyramid	2.712	60	
3	6	$\text{Cp}^*_2\text{Ru}_2\text{B}_4\text{H}_8$	Capped tetragonal pyramid	2.855	50	Capped tetragonal pyramid	2.828	60	
4		$\text{Cp}^*_2\text{Re}_2\text{B}_4\text{H}_8$	Bicapped tetrahedron	2.809	52	Bicapped tetrahedron	2.832	60	
5	7	$\text{Cp}^*_2\text{Mo}_2\text{B}_5\text{H}_9$	Bicapped trigonal bipyramid	2.809	54,55,6 1	Bicapped trigonal bipyramid	2.802	62	
6		$\text{Cp}^*_2\text{W}_2\text{B}_5\text{H}_9$	Bicapped trigonal bipyramid	2.817	56	Bicapped trigonal bipyramid	2.836	62	
7	8	$\text{Cp}^*_2\text{Rh}_2\text{B}_6\text{H}_{10}$	B_8H_{12}	3.850	57	B_8H_{12}	3.858	63	
8		$\text{Cp}^*_2\text{W}_2\text{B}_6\text{H}_{10}$	Bicapped octahedron	2.959	58	Bicapped octahedron	2.970	63	

Predicted metallaborane structures confirmed *a posteriori* by experiments

The first experimental study concerning the synthesis of novel hydrogen-rich dimetallaboranes (i.e. structures that were not experimentally known when the results of our computations were published) appeared in 2017 in the journal *Inorganic Chemistry*.⁶⁴ Here, the eight-vertices Ir complex, $\text{Cp}^*_2\text{Ir}_2\text{B}_6\text{H}_{10}$, was synthesized and its structure was characterized by

X-ray crystallography and NMR investigations. The experimentally obtained crystal structure corresponds to our $\text{Ir}_2\text{B}_6\text{-1} \leftrightarrow \text{Ir}_2\text{B}_6\text{-2}$ fluxional ground state that was computed in our 2016-published *Dalton Transactions* paper.⁶³ The crystal structure revealed that, similar to its Rh counterpart, $\text{Cp}^*_2\text{Ir}_2\text{B}_6\text{H}_{10}$ adopts the geometry of the B_8H_{12} molecule and has its metal vertices placed in opposing vertices. The bridging H atoms that were shown in our study to cause a fluxionality of the ground state by their movement on the polyhedron's open face were found to be terminal atoms connected to the Ir vertices. This might not come as a big surprise since our predicted structures were computed in gas-phase while the experiments were done in solution and solid state. Thus, the minute energy difference between the states related with different positions of the bridging H atoms that appears in gas-phase can be removed in solution due to the molecule's interaction with the surrounding medium.

Table 2. *A posteriori* determined structures and their corresponding computed ground states.

#	V	Computationally predicted structure				A posteriori experimentally determined		
		Metallaborane	Geometry	M-M (Å)	Ref.	Geometry	M-M (Å)	Ref.
1	6	$\text{Cp}^*_2\text{Mo}_2\text{B}_4\text{H}_8$	Bicapped tetrahedron	2.997	60	Bicapped tetrahedron	N/A	65
2		$\text{Cp}^*_2\text{W}_2\text{B}_4\text{H}_8$	Bicapped tetrahedron	2.632	60	Bicapped tetrahedron	N/A	65
3	8	$\text{Cp}^*_2\text{Ir}_2\text{B}_6\text{H}_{10}$	B_8H_{12}	3.883	63	B_8H_{12}	3.851	64

The second study that experimentally investigated some previous unknown hydrogen-rich dimetallaboranes appeared in 2018 in the journal *Organometallics*.⁶⁵ The authors managed to synthesize the Mo and W six vertices systems, i.e the $\text{Cp}^*_2\text{M}_2\text{B}_4\text{H}_x$ with $x = 8$ or 10 . The authors claim to have obtained the hydrogen saturated $\text{Cp}^*_2\text{M}_2\text{B}_4\text{H}_{10}$ $M = \text{Mo}, \text{W}$ (i.e. with 6 “extra” H atoms) and not the $\text{Cp}^*_2\text{M}_2\text{B}_4\text{H}_8$ ($M = \text{Mo}, \text{W}$) which was the expected⁶⁶ intermediate in their studied reaction. However, due to the experimental limitation, no direct evidence of the actual obtained hydrogen-rich metallaborane could be provided. The claim of their study relies on the structural determination of a precursor of the $\text{Cp}^*_2\text{M}_2\text{B}_4\text{H}_x$ with $x = 8 - 10$, the $(\text{Cp}^*\text{MCO})_2\text{B}_4\text{H}_6$. Their entire argument relies on the implicit assumption that, once the two CO groups depart from the cluster, the generated 4 electron gap should be balanced by 4 electrons donated by 4 incoming extra H atoms. Hence, they conclude, the total number H atoms of the

molecular formula should be 10. However, the authors fail to acknowledge that by no means the addition of 4 extra H atoms is the only way by which the cluster can balance its 4 electron deficiency caused by the leaving of the 2 CO units. More likely, the cluster will form a double M=M bond (yielding extra 2 electrons for cluster bonding) and coordinate only 2 extra H atoms (that donate the remaining 2 electrons that are required). The presence of M=M (M = Mo, W) double bonds in the $\text{Cp}^*_2\text{M}_2\text{B}_4\text{H}_8$ (M = Mo, W) were already predicted by our study relating these systems.⁶⁰ Furthermore, the formation of this extra double bond is also clearly stated by their computational results. As this leads to the contradiction of claim, the authors simply ignore the outcome of this result.

The higher so-called thermodynamic stability of $\text{Cp}^*_2\text{M}_2\text{B}_4\text{H}_{10}$ based on the higher HOMO-LUMO gap is an artificial argument. The implied stability is actually the chemical stability of the molecule and gives no information about the thermodynamics of the formation reaction. The HOMO-LUMO gap provides information regarding the molecule's reactivity and not about its formation.

Starting from the CO-devoid cluster, the Mo system will have to pass through the H8 format in order to arrive at the H10 variant. We already know that the H8 structure is the ground state of the Mo systems and thus it is expected that addition of the extra 2 H would require an energetic cost in order to pass through transition state.

Thus, it is not clear which of the candidates is actually the intermediate. Either way, its core structure is the one predicted by us. The experimentalists provide no conclusive proof that H10 is what they found.

Table 3. Skeletal electron count of the $(\text{CpMoCO})_2\text{B}_4\text{H}_6$, $\text{Cp}_2\text{Mo}_2\text{B}_4\text{H}_8$ and $\text{Cp}_2\text{Mo}_2\text{B}_4\text{H}_{10}$ molecules.

Molecule	Fragment	Nr. of fragments	e ⁻ donated by fragment	Total e ⁻ donated
$(\text{CpMoCO})_2\text{B}_4\text{H}_6$	CpMo	2	6-6-1=-1	-2
	BH	4	2	8
	H	2	1	2
	CO	2	2	4
	Mo=Mo	0	2	0
Skeletal electron count				12
$\text{Cp}_2\text{Mo}_2\text{B}_4\text{H}_8$	CpMo	2	6-6-1=-1	-2
	BH	4	2	8
	H	4	1	4
	CO	0	2	0
	Mo=Mo	1	2	2
Skeletal electron count				12
$\text{Cp}_2\text{Mo}_2\text{B}_4\text{H}_{10}$	CpMo	2	6-6-1=-1	-2
	BH	4	2	8
	H	6	1	6
	CO	0	2	0
	Mo=Mo	0	2	2
Skeletal electron count				12

Chapter Conclusions

Between 2014 and 2016 we published 4 papers regarding the structures of the five vertices,⁵⁹ six vertices,⁶⁰ seven vertices⁶² and eight vertices⁶³ hydrogen-rich dimetallaboranes of the Pt, Pd, Rh, Ir, Ru, Os, Re, Mo, W and Ta transition metals, rationalizing their isomer hypersurface and indicating correlations between ground state preferences and classical structural rules such as Wade-Mingos. Out of the 34 predicted structures, 8 structures were experimentally known at the time of our publication (cf. Table 1.) and were found by our computation to be ground states in their corresponding potential energy surfaces.

Following the publications of our results, two experimental papers that were concerned with the synthesis of hydrogen-rich metallaboranes structures similar to those investigated in this chapter appeared in the journals *Inorganic Chemistry*⁶⁴ and *Organometallics*⁶⁵. Here, the

structures of the 6-vertices $\text{Cp}^*_2\text{Mo}_2\text{B}_4\text{H}_8$ and $\text{Cp}^*_2\text{W}_2\text{B}_4\text{H}_8$ alongside the 8-vertices $\text{Cp}^*_2\text{Ir}_2\text{B}_6\text{H}_{10}$ molecules were determined. These experimentally determined structures confirmed our $\text{Cp}_2\text{Mo}_2\text{B}_4\text{H}_8$,⁶⁰ $\text{Cp}_2\text{W}_2\text{B}_4\text{H}_8$ ⁶⁰ and $\text{Cp}_2\text{Ir}_2\text{B}_6\text{H}_{10}$ ⁶³ predicted structures .

4 Theoretical investigations of the sulfite reductase active site

Pars energetica: The importance of the siroheme modification

Sulfite reductase (SiR) is a siroheme-containing metalloenzyme that catalyzes the reduction of sulfite (SO_3^{2-}) to species containing sulfur in a lower oxidation state, such as sulfide (S^{2-} or SH^-), trithionite ($\text{S}_3\text{O}_6^{2-}$) or thiosulfate ($\text{S}_2\text{O}_3^{2-}$),^{67,68} involving up to six electrons. Based on the usage of the reaction product, SiR enzymes can be classified as assimilatory (when sulfide is prepared for the incorporation into sulfur-containing amino acids and cofactors) or dissimilatory (when sulfite is used as an electron acceptor in the final reductive step of anaerobic respiration processes). Assimilatory sulfite reductases (ASiR) have a $\alpha\beta\gamma$ heterotrimeric structure, feature sulfide as final reaction product and are found in bacteria, archaeobacteria, fungi and plants. On the other hand, the dissimilatory SiR (DSiR) have a $\alpha_2\beta_2$ heterotetrameric structure, can reduce sulfite to either trithionite or thiosulfate and are found in eubacteria and archaeobacteria.⁶⁹ While ASiR and DSiR differ in terms of structure and product of reduction, they have the same type of active site, comprised of a variant of heme that belongs to the isobacteriochlorin class, named siroheme, connected via an endogenous cysteine residue to an Fe_4S_4 cubane. Siroheme differs from heme in that it contains two double bonds less, reducing the amount of conjugation of the ring system. The electrons required for sulfite reduction in SiR are provided by flavoproteins and are initially funneled to the iron–sulfur cubanes that further transmit them to the siroheme iron, to which substrate is bound and subsequently reduced.⁷⁰ In addition to its catalytic activity, SiR is also known to play an important role in compacting nucleoids in plastids by binding to chloroplast DNA,⁷¹ possibly acting as a sensor of the chloroplast's redox state, as protector of DNA against oxidative damage⁷² or global regulator of nucleoid transcription⁷³ and replication.⁷⁴

In ASiR, the active site is close to the surface, at the interface of the three monomers.⁷⁵ As seen in Figure 14, the siroheme is located in a surface-exposed hydrophilic cavity, with its equatorial side facing the solvent. The distal side of the heme is lined with hydrophilic amino acids that help binding the substrate, sulfite (in crystal structures, this position is often occupied

by a phosphate group, as in Figure 14). On the proximal side of the heme, a cysteine residue bridges it to the cubane cofactor, which is not exposed to the solvent.

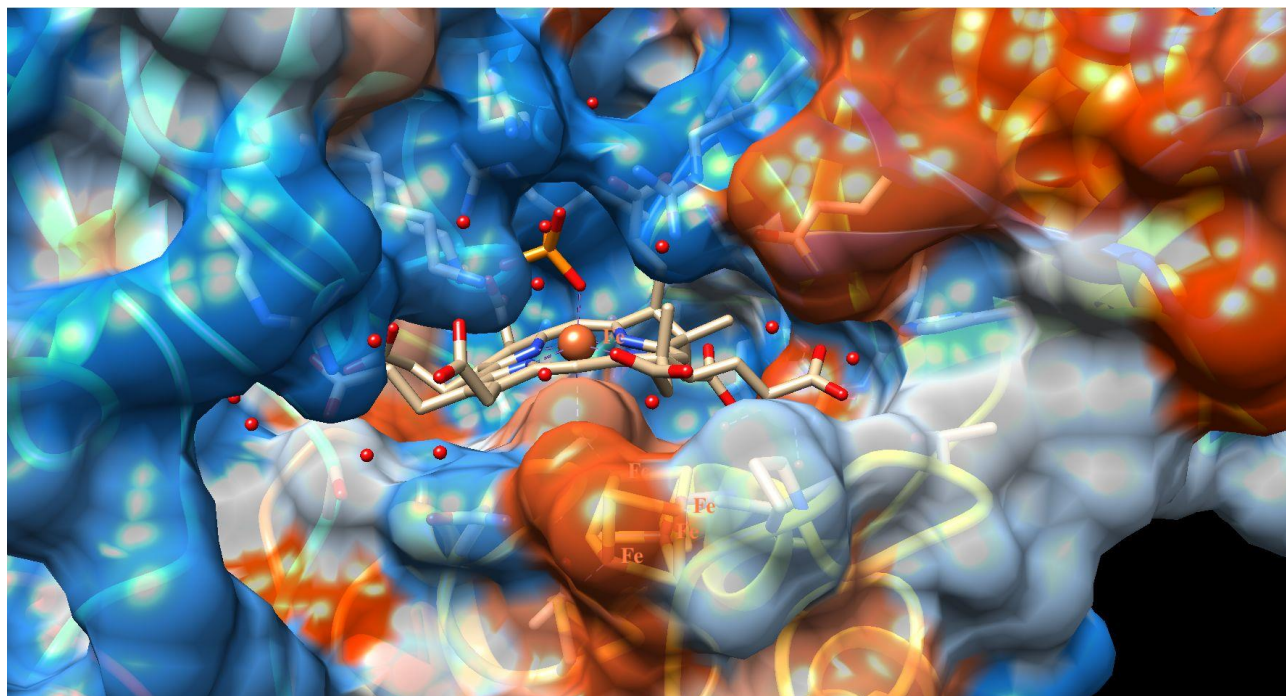


Figure 14. The ASiR active site. The amino acid side-chains are in ribbon representation with hydrophobic areas shaded in red and hydrophilic areas in blue; the siroheme is shown in stick representation. A phosphate group, as found in the enzyme's resting state, is located in a hydrophilic pocket found on the distal side of heme. The cubane cofactor, also represented in a stick manner, is buried in the enzyme. Red dots represent water molecules.

EPR measurements of the SiR active site in its resting-state reveal a high-spin ferric species ($S = 5/2$) associated with the siroheme center, which can be reduced to the high-spin ferrous state ($S = 2$) at a redox potential of -340 mV.⁷⁶ The EPR-silent Fe_4S_4 center was shown in Mössbauer spectra⁷⁷ to feature an antiferromagnetic interaction between two faces of the cubane. On each face resides a high spin ferrous ion ferromagnetically coupled to a ferric ion, adding up to a local spin $S = 9/2$ on one side and $-9/2$ on the other side. A schematic representation of SiR active site magnetic alignment is provided in Figure 15, where the orientation of the excess spin located on each iron ion is represented by a black arrow. The cubane cluster core has a 2+ charge in this oxidized resting state, and total charge of 2- after including the $4(\text{SR})^-$ cysteine anion ligands.

The catalytic mechanism of SiR has been explored experimentally^{67,78} and computationally.^{79–82} However, the previous computational studies did not provide a quantitative account of the importance of the siroheme group (compared to heme), nor on the effect or participation of the coupled Fe₄S₄ cubane on the reactivity of the siroheme. On the other hand, standalone iron–sulfur cubane systems have themselves been studied extensively in both computational^{83,84} and joint experimental and theoretical investigations.^{85–88} Furthermore, the active site of [FeFe] hydrogenases, in which a cubane is directly connected via a cysteinate to a diiron catalytic core (as opposed to a heme in SiR), has also been subject to previous research.^{89–}

93

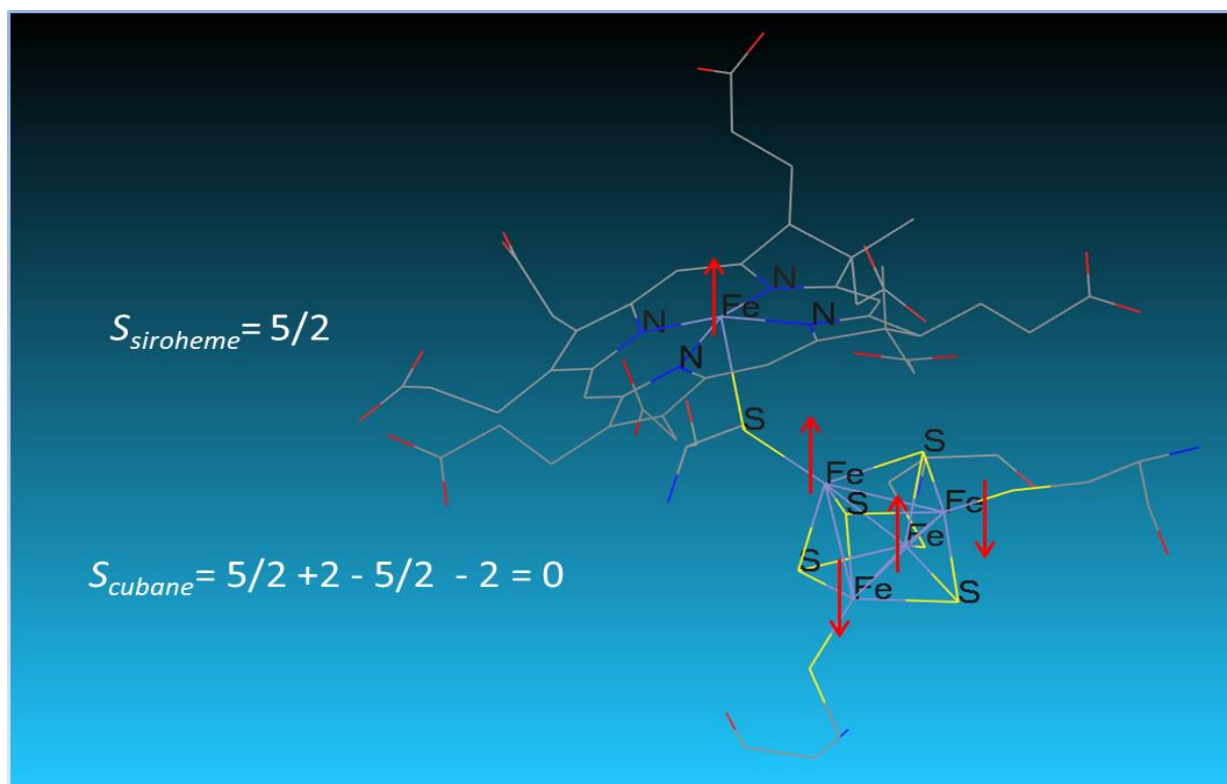


Figure 15. The SiR oxidized active site comprised of a siroheme factor (upper half) connected via a cysteine sulfide (middle) to a Fe₄S₄²⁺ cofactor (lower half). Red arrows represent the orientation of the local majority spin population found on each iron ion. The figure shows one of the six possible broken-symmetry solutions that yields a total sextet located on the siroheme. Carbon atoms are depicted in grey, sulfur in yellow, oxygen in red, nitrogen in blue and iron in violet.

Besides enzymes that are involved in its own biosynthesis⁹⁴⁻⁹⁷, siroheme is never present alone in any enzyme active site: it is always coupled to an iron-sulfur cluster.^{78,98-100} Conversely, there are no examples of cubanes coupled to other types of heme in proteins, even though heme groups and iron-sulfur centers often occur together in electron transfer (for example, formate dehydrogenase-N¹⁰¹ has a 90-Å long chain of redox centers involving molybdopterin-guanine dinucleotides, menaquinone, five Fe₄S₄ cubanes and two hemes; interestingly, the iron-sulfur cubanes in this case are situated along the heme plane, whereas in SiR the iron-sulfur cubane is aligned perpendicular to the siroheme). However, synthetic variants of heme-cubane systems have been constructed. While in earlier attempts no sign of catalytic activity was observed,^{102,103} it was recently shown that by tuning the first sphere of interaction such that the SiR environment is reproduced, the heme-cubane system could catalyze the sulfite reduction similarly to the native, siroheme-cubane version of SiR active site.¹⁰⁴ Thus, by showing that siroheme is not crucial for SiR to properly function, it became even more intriguing why this enzyme employs siroheme and not the ubiquitous heme cofactor.

The effect of this siroheme modification within the SiR active site, as well the effect of the cubane on the (siro)heme system (spin-state accessibility, energetic and bond order change of the siroheme-cysteine interaction, or influence on the reaction mechanism) thus remain to be fully explored. Possible hypotheses include the control of the spin state of the substrate-binding (siro)heme iron, modulation of the trans effect of the (Fe₄S₄-bound) cysteinylate, or modulation of the redox potential. Therefore, in the present study, these issues are explored using DFT methodology. However, finding a computational protocol that performs acceptably in all spin-state situations encountered in complex systems with multiple magnetic interactions and multiple redox isomerism opportunities such as SiR is not a trivial task. Hence, a benchmark test of several density functional methods was performed using a set of four bioinorganic centers, with emphasis on the difficult issue of correctly predicting spin-state preference as well as geometry. Then, a detailed description of the SiR active site models is given, investigating the available spin states and redox potentials of the (siro)heme centers, as well as the interaction of the two cofactors in terms of energy decomposition analysis (EDA)^{105,106} and Mayer bond-order (MBO)¹⁰⁷ analysis.

Models that describe the sulfite reductase (SiR) active site were employed in a computational investigation in order to assess the role of the cubane [4Fe-4S] cubane and the modified siroheme structure adapted by the SiR on the properties of its active site. In order to find a suitable DFT method that can handle the challenging electronic structure associated with the SiR active site, eleven DFT functionals were tested on four iron-containing biologically-relevant active site models. The B97-D, B3LYP and M06-L functionals offered the best performance and the latter two were further employed in (siro)heme computations.

In conclusion, by substituting heme with siroheme, crucial aspects related to the SiR functionality are affected. By reducing the porphyrin conjugation, the ligand field interactions between the central Fe and the surrounding N atoms are decreased in siroheme systems. Corroborated with the asymmetric distribution of charge among the N atoms, this leads to a stabilization of the high-spin states associated with the porphyrin Fe. Furthermore, the redox potential of this center becomes more negative. The effect induced by the siroheme on the interfactor bond is, however, is antagonistic depending on the iron oxidation state: while it becomes stronger in the ferrous systems, it weakens in ferric ones.

Pars ballistica: Why does sulfite reductase employ siroheme?

As also discussed in the previous sections, although heme and cubane groups are known to be simultaneously used by some enzymes,¹⁰¹ the two cofactors are never covalently connected to each other directly – with the exception of the SiR active site, where a cysteine thiolate bridges one cubane Fe ion to the siroheme. Conversely, siroheme is never present alone in any enzyme active site (besides in enzymes involved in its own biosynthesis) – it is always coupled to a cubane iron–sulfur cluster.^{78,98–100} While the prime role of the cubane in the SiR mechanism is to provide electrons for the reaction (six electrons are needed to reduce sulfite to S^{2-}), the choice of siroheme vs. heme in SiR has not been rationalized until the work reported in the present thesis.

In this chapter, we study how siroheme modifies the electron-transfer properties of the SiR active site compared to heme by using computational methods, providing a plausible explanation why SiR uses siroheme rather than heme.

By treating the SiR active site as a molecular junction (cf. Figure 16), the non-equilibrium Green's function coupled with density functional theory (NEGF-DFT) framework can be employed to compute its electron-transport properties.^{156,158,166} Using this approach, an electron-route analysis was performed on four routes by which electrons can be transferred from the cubane to the (siro)heme cofactor (cf. Figure 17).

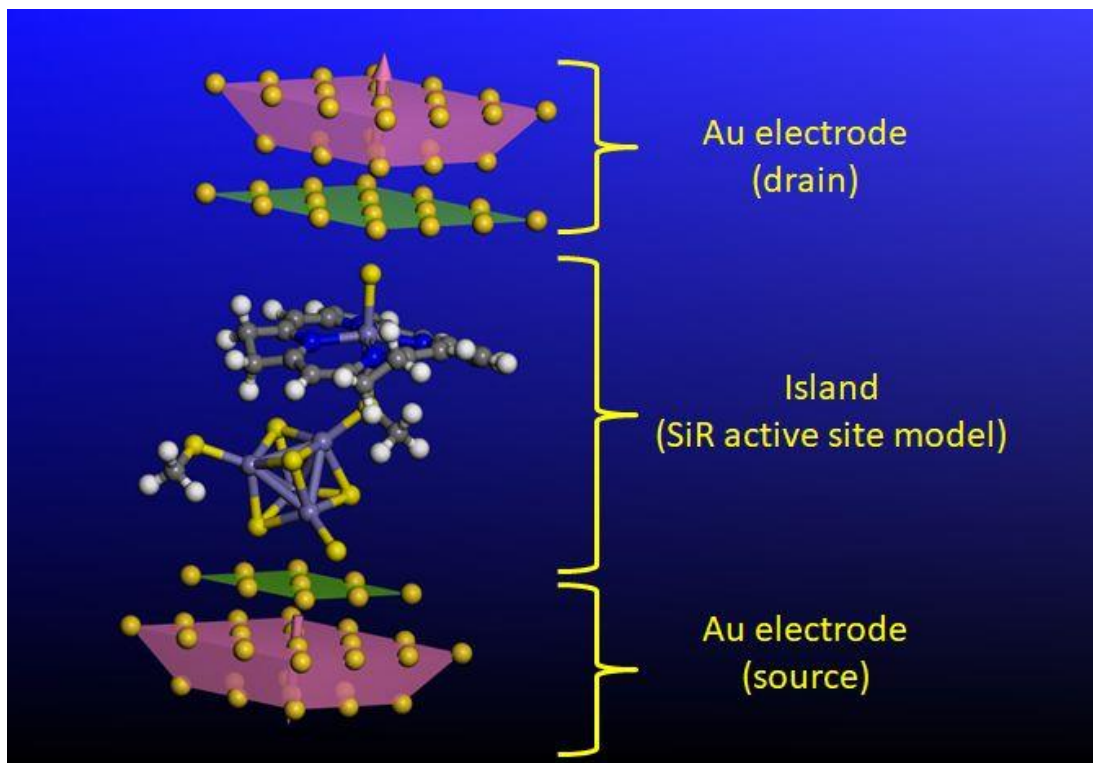


Figure 16. SiR active site as a molecular junctions connecting two Au electrodes. Au atoms are depicted in dark yellow, Fe in violet, N in blue, S in yellow, O in red, C in grey and H in white.

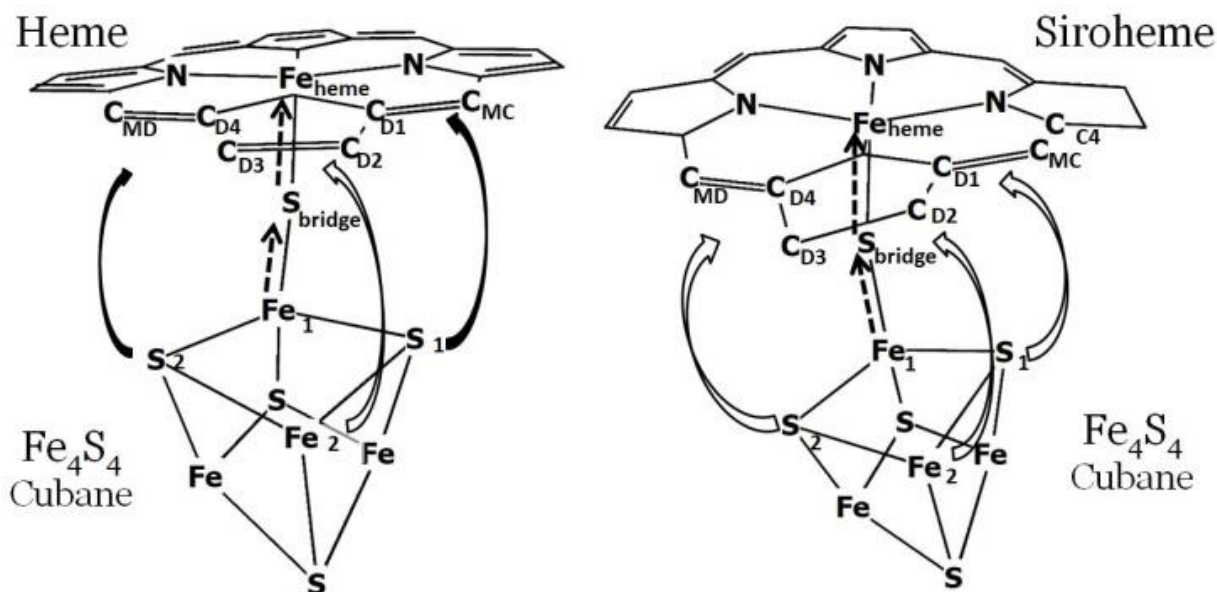


Figure 17. Electron routes investigated in the heme–cubane (left) and siroheme–cubane systems (right). The bridged route is depicted with dashed arrows, while the direct routes are shown with solid arrows. High conductance is depicted in black, while low conductance is in white.

Siroheme tunes the electron transfer from the cubane cofactor to the substrate such that, when compared to the heme variant of the SiR active site, the states associated with the through-vacuum charge transfer are inhibited, while the states involved in the through-bridge charge transfer are modified to increase the electron transmission (cf. Figure 18). Thus, the role of siroheme is to block the delaying porphyrin \rightarrow Fe_{heme} step in order to increase the overall charge transfer from the cubane cofactor. Furthermore, siroheme reduces the risk of porphyrin acquiring partial radical character that comes as an effect of the electrons being transmitted from the cubane via routes that involve the periphery of the porphyrin π -system. By avoiding these charge-transfer channels, the macrocycle is protected against undesired radical attack.

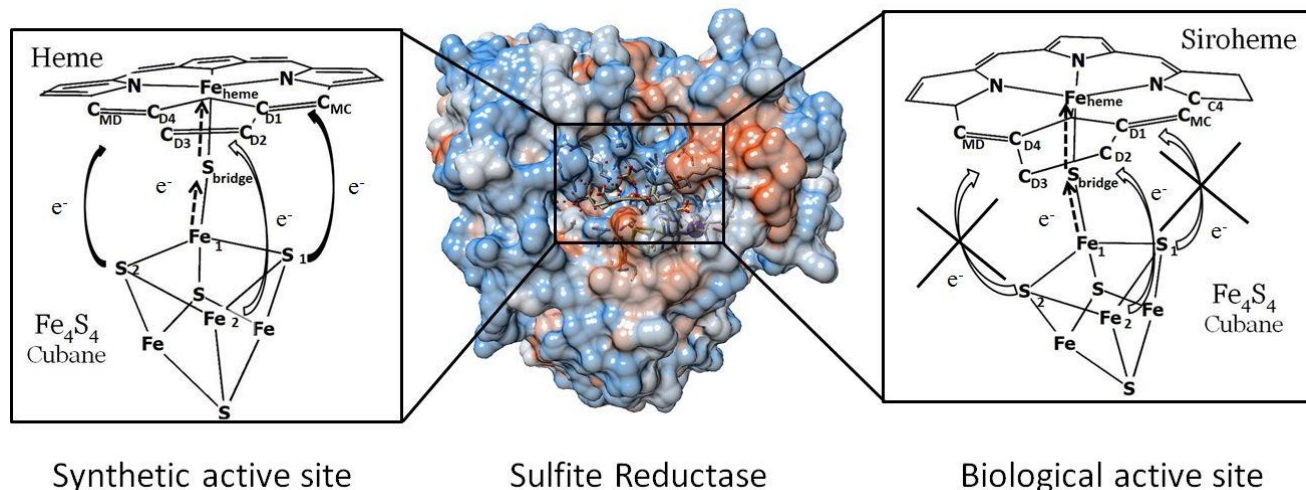


Figure 18. As opposed to heme, siroheme inhibits the charge transfer from the cubane via direct routes.

Pars mechanistica: SiR reaction mechanism

The reaction mechanism by which SiR reduces sulfite (SO_3^{2-}) to sulfide (S^{2-}) has previously been proposed⁸² based on experimental data regarding the known intermediates and by complementing the known information with computational obtained data of the experimentally unseen intermediates. However, this previously proposed SiR reaction mechanism was built based on models of intermediates that completely neglected the cubane cofactor. In order to afford the computational cost that the full active site required, it was assumed that the role of the cubane cofactor within the SiR active site is restricted to providing electrons and does not influence the reaction mechanism. In this chapter we extend the computational endeavor upon this mechanism and provide new insights to its functioning. We start by recomputing these cubane-less models at a DFT level that will make the results coherent with the rest of this chapter. We then incorporate models that contain the cubane cofactor but also an intermediate set of models in which the $[\text{Fe}_4\text{S}_4]^{2+}$ cofactor is replaced by a diamagnetic Zn^{2+} ion. This allows the differentiation of the magnetic and metallic influence of the *trans effect* on the reaction mechanism. Furthermore, different electronic states are assigned to each model and also the bond isomerism (where possible) is investigated. The outcome of this endeavor is outlined in Figure 23.

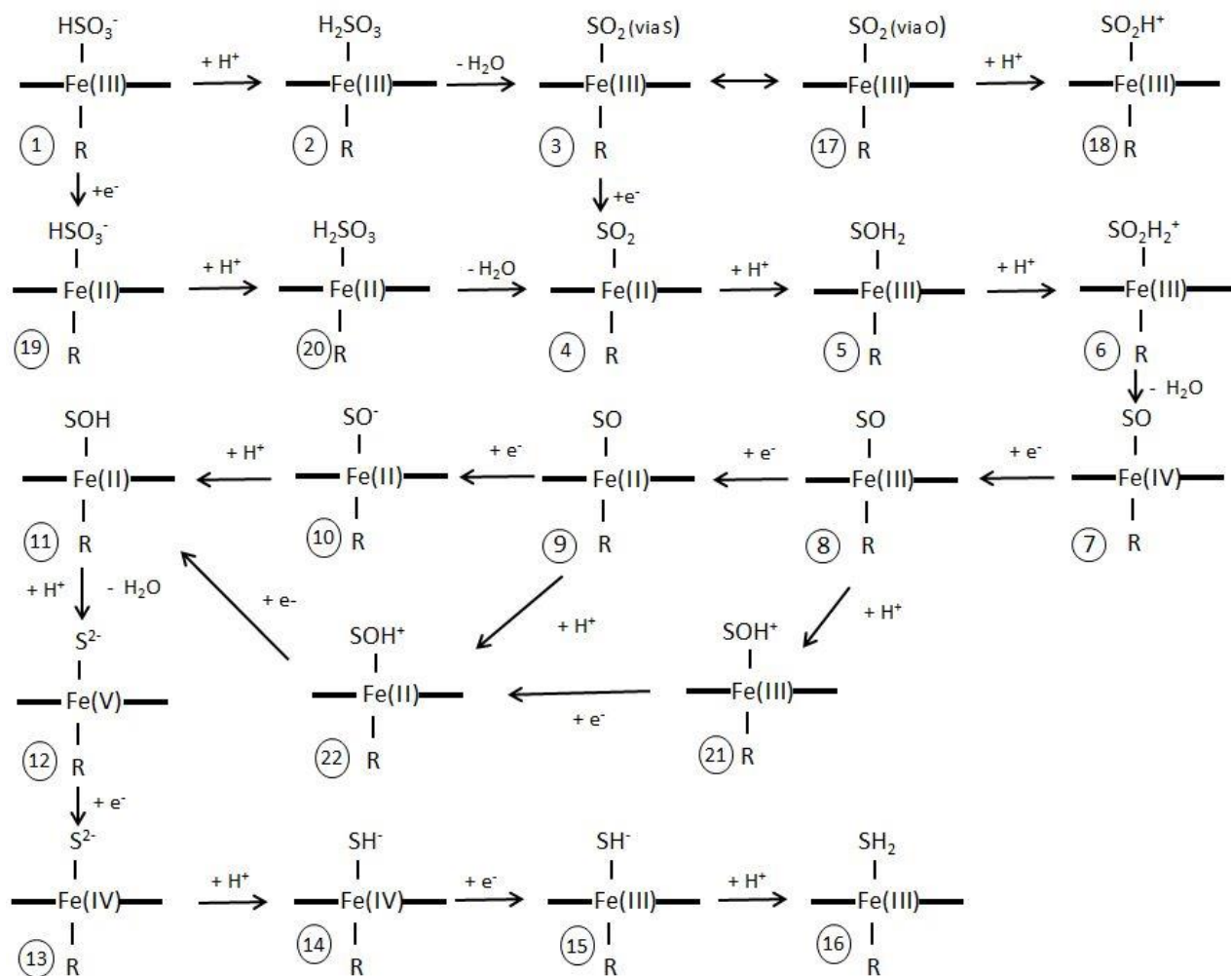


Figure 19. SiR reaction mechanism.

Chapter Conclusions

We have shown that the specific porphyrin modification that the siroheme possesses, compared to the ubiquitous heme, induces effects that can be exploited by the sulfite reductase enzyme. We have first shown that by reducing its ring conjugation, siroheme reduces the ligand field interaction between its central Fe atom and the vicinal N atoms. The distribution of charge on the latter atoms becomes asymmetrical, the ligand-ligand and ligand-metal distances are increased and overall all these aspects lead to a better accommodation of the high-spin Fe species

within the porphyrin ring. Also, the reduction potential of the siroheme Fe becomes more negative. The *Pars energetica: The importance of the siroheme modification* subchapter dealing with these *διάνοια* aspects has been published in the Journal of Inorganic Biochemistry.¹⁷⁷

A *διάνοια* → *επιστήμη* transition has been made in the following subchapter. Here it was shown that the ultimate reason behind SiR's siroheme adoption lies in the latter's tuning capabilities of the electron transfer incoming from the cubane cofactor. Thus, by inhibiting routes that imply the edge of the porphyrin, the charge transfer rate from the cubane to the central Fe_{siroheme} is increased and the porphyrin is kept in a radical-free state that, in turn, makes it less susceptible in reacting with radical intermediates and solvent molecules. The *Pars ballistica: Why does sulfite reductase employ siroheme?* subchapter dealing with this *επιστήμη* result was published in the Chemical Communications journal.¹⁸⁰

The cubane cofactor was also shown to influence the SiR reaction mechanism. Thus, besides providing the electrons needed for substrate reduction, the cubane also stabilizes the SiR intermediates and in some cases corrects the binding of adducts that are likely to employ linkage isomerism. By promoting the substrate to bind via the S atom to the (siro)heme, the sulfur is retained at the active site until it is fully reduced at the end of the catalytic cycle. The obtained results of the *Pars mechanistica: SiR reaction mechanism* subchapter are currently prepared for publication; so far, we have published a paper on a very small number of the clusterless intermediate models.⁸⁰

5 Epilogue

During the PhD period we have managed to publish 9 articles, cited 18 times. Our most recent one, the *ChemComm* paper, after just three months since its publication, was cited¹⁸¹ by a review article when discussing the siroheme prosthetic group (as reason for its adoption).

The driving force behind this thesis' start was the understanding of the chemical bond. We have come to understand that the chemical bond belongs to that class of things that are not. Consequently, all other *unicorns*¹⁸² derived from it, such as resonance, conjugation, hyperconjugation, covalent bonding, donor-acceptor bond, agostic interactions, π bonding etc, share the same non-existence. From the quantum mechanical point of view, chemical bonds simply do not exist, as no operator is associated with this quantity and therefore no observable quantity either. At best, chemical bond information is chopped out of the wavefunction. It is far more accurate to state that the chemical bond is an *εικόν* of the wavefunction: it is the outcome of the wavefunction projection unto the chemical language. Deeper reasoning (cf. section 2.4.3.2.1.) implies their viewing as local, stabilized, Fermi heaps. In general, a chemical system is better seen as an electronic density disturbed by the presence of positive nuclei. The fundamental disturbance caused by the doping of the electronic density with positive point-like nuclei is found in the system's energetic behavior: if in the absence of nuclei the electrons adopted a continuous range of energetic states, in their presence the electrons will adopt a discrete range of energetic states. This, corroborated with symmetry requirements imposed by Pauli's spin statistics, marks the point from where chemistry commence.

To emphasize the illusory character that the traditional chemical bond concept possesses we will further compare it, in a ludic manner, with the *Battle of the 300 Champions*. Fought in 546 BC between the Greek city-states of Argos and Sparta, this battle has a disputed outcome as both belligerents claimed victory at its end. Instead of engaging in a full strength battle, the combatant armies agreed to each deploy their 300 best soldiers in a death match in which victory would be acclaimed by the side that at the end of the battle will have surviving soldiers that could tell the outcome. Both armies retreated to their cities (so that neither side could interfere in the battles itself) and the 600 champions were left alone to fight on the field of Thyrea. At the end of the battle there were only two Argos soldiers still standing - and they consequently retreated home acclaiming victory. What they overlooked, however, was an injured Spartan that,

after seeing them gone, managed to survive enough to reach home and thus claim victory as well. Claiming that the chemical bond, for instance, in the O_2 molecule is the outcome of 4 electrons forming two covalent bonds is similar to stating that the Battle of the 300 Champions was fought by the 3 surviving hoplites. In both cases, the contribution of other electrons/hoplites is neglected. Similar to how the outcome of the battle is a consequence of shed blood, so is the chemical bond a consequence of annihilated wavefunction. The electronic density present between the two O atoms forming the O_2 molecule exceeds by far the amount required by the presence of 4 electrons. The non manifesting excess simply annihilates itself by having opposing wavefunction sign in that region. But this does not mean that it is not there; its manifestation in terms of what we called chemical bond is simply canceled out. Assigning a O=O bond to the O_2 molecule resembles the forgotten blood of what became nameless soldiers that fought at Thyrea, while the “=” in O=O resembles the remembered names of surviving soldiers. Indeed, an anthropic behavior and therefore nothing more than an anthropic construct.

In the spirit of this chapter’s motto, we will not speak of things not finished but rather just mention them as directions for future studies. Thus, our further studies, sprung from this thesis, are two folded. On the metallaborane perspective, we have in preparation results of the 9 and 10 vertices containing systems. Furthermore, we intend to investigate their possible applicability as single-molecular junctions. On the sulfite reductase perspective, we have in preparation a *Pars magnetica* investigation in which the interfactorial magnetic interactions are studied. Furthermore, we plan to investigate the effect that the siroheme modification has on the interfactorial quantum entanglement. Also, a line of study is in work, where sulfite reactions with systems related to the (siro)heme are investigated at the DFT level – in collaboration with experimentalists. These are prospects that we look forward to further exploring, both because of their practical implications and because of the challenges they offer on a fundamental level and which in themselves offer strong motivation to those sharing a passion in science even when the practical applications are not immediately forthcoming; after all, as once said by Bertrand Russell, *there is much pleasure to be gained from useless knowledge.*

6 Thesis references

1. B. E. Sernelius, *Int. J. Mod. Phys. A*, **2009**, 24, 1804–1812.
2. D. Frauchiger and R. Renner, *Nat. Commun.*, **2018**, 9, 1–10.
3. V. R. I. Kaila, *J. R. Soc. Interface*, **2018**, 15.
4. P. Pyykko and J. P. Desclaux, *Acc. Chem. Res.*, **1979**, 12, 276–281.
5. G. Gamow, *Nature*, **1928**, 122, 805–806.
6. R. B. King, *Chem. Rev.*, **2001**, 101, 1119–1152.
7. A. Stock, *Hydrides of boron and silicon*, Cornell University Press, Ithaca, NY, **1933**.
8. W. Dilthey, *Zeitschrift für Angew. Chemie*, **1921**, 34, 596.
9. H. C. Longuet-Higgins, *Proc. Roy. Soc.*, **1945**, 183, 357.
10. W. N. Lipscomb, *Boron Hydrides*, W. A. Benjamin, New York, **1963**.
11. K. Hedberg and V. Schomaker, *J. Am. Chem. Soc.*, **1951**, 73, 1482–1487.
12. K. S. Pitzer, *J. Am. Chem. Soc.*, **1945**, 67, 1126–1132.
13. W. H. Eberhardt, B. Crawford and W. N. Lipscomb, *J. Chem. Phys.*, **1954**, 22, 989–1001.
14. R. E. Williams, *Inorg. Chem.*, **1971**, 10, 210–214.
15. H. C. Longuet-Higgins and M. de V. Roberts, *Proc. R. Soc. London. Ser. A. Math. Phys. Sci.*, **1955**, 230, 110–119.
16. A. R. Pitochelli and M. F. Hawthorne, *J. Am. Chem. Soc.*, **1960**, 82, 3228–3229.
17. M. F. Hawthorne and A. R. Pitochelli, *J. Am. Chem. Soc.*, **1959**, 81, 5519.
18. J. A. Wunderlich and W. N. Lipscomb, *J. Am. Chem. Soc.*, **1960**, 82, 4427–4428.
19. A. Kaczmarczyk, R. D. Dobrott and W. N. Lipscomb, *Proc. Natl. Acad. Sci.*, **1962**, 48, 729–733.
20. F. Klanberg, D. R. Eaton, L. J. Guggenberger and E. L. Muetterties, *Inorg. Chem.*, **1967**, 6, 1271.
21. R. B. King and A. J. W. Duijvestijn, *Inorganica Chim. Acta*, **1990**, 178, 55–57.
22. I. Shapiro, D. C. Good and R. E. Williams, **1962**, 84, 3837.
23. I. Shapiro, R. E. Williams and D. C. Good, *J. Am. Chem. Soc.*, **1963**, 3167–3171.
24. R. B. King and D. H. Rouvray, *J. Am. Chem. Soc.*, **1977**, 99, 7834–7840.
25. J. Aihara, *J. Am. Chem. Soc.*, **1978**, 100, 3339–3342.
26. A. J. Stone and M. J. Alderton, *Inorg. Chem.*, **1982**, 21, 2297–2302.
27. K. Wade, *Chem. Commun.*, **1971**.
28. D. M. P. Mingos, *Acc. Chem. Res.*, **1984**, 17, 311–319.
29. R. Hoffman, *Angew. Chem. Int. Ed.*, **1982**, 27, 711–800.
30. J. D. Kennedy, *The Borane-Carborane-Carbocation Continuum*, Wiley, New York, **1998**.
31. S. Ghosh, M. Shang, Y. Li and T. P. Fehlner, *Angew. Chem. Int. Ed.*, **2001**, 40, 1125–1128.
32. R. B. King, *Inorg. Chem.*, **2006**.
33. S. H. Vosko, L. Wilk and M. Nusair, *Can. J. Phys.*, **1980**, 58, 1200–1211.
34. A. D. Becke, *J. Chem. Phys.*, **1993**, 98, 5648–5652.
35. C. Lee, W. Yang and R. G. Parr, *Phys. Rev. B*, **1988**, 37, 785–789.
36. D. Andrae, U. Häußermann, M. Dolg, H. Stoll and H. Preuß, *Theor. Chim. Acta*, **1990**, 77, 123–141.
37. Y. Zhao and D. G. Truhlar, *Theor. Chem. Acc.*, **2008**, 120, 215–241.
38. P. J. Stephens, F. J. Devlin, C. F. Chabalowski and M. J. Frisch, *J. Phys. Chem.*, **1994**, 98, 11623–11627.
39. 2013 Frisch, M. J. et al. Gaussian 09, Revision E.01, Gaussian, Inc., Wallingford CT, .

40. F. Weinhold and C. R. Landis, *Valency and Bonding: A Natural Bond Order Donor-Acceptor Perspective*, Cambridge University Press, Cambridge, **2005**.
41. A. Lupan and R. Bruce King, *Inorganica Chim. Acta*, **2013**, 397, 83–87.
42. H. Wang, Y. Xie, R. B. King and H. F. Schaefer, *J. Am. Chem. Soc.*, **2006**, 128, 11376–11384.
43. E. A. McNeill, K. L. Gallaher, F. R. Scholer and S. H. Bauer, *Inorg. Chem.*, **1973**, 12, 2108.
44. P. T. Brain, D. Hnyk, D. W. H. Rankin, M. Bühl and P. von Ragué Schleyer, *Polyhedron*, **1994**.
45. H. Yan, A. M. Beatty and T. P. Fehlner, *Organometallics*, **2002**, 21, 5029–5037.
46. A. Lupan and R. B. King, *Inorg. Chem.*, **2012**, 51, 7609–7616.
47. A. Lupan and R. B. King, *Organometallics*, **2013**, 32, 4002–4008.
48. X. Lei, M. Shang and T. P. Fehlner, *Chem. - A Eur. J.*, **2006**, 6, 2653.
49. X. Lei, M. Shang and T. P. Fehlner, *Organometallics*, **2000**, 19, 118–120.
50. X. Lei, M. Shang and T. P. Fehlner, *J. Am. Chem. Soc.*, **1999**, 121, 1275–1287.
51. R. Mason, K. M. Thomas and D. M. P. Mingos, **1973**, 95, 3802–3804.
52. S. Ghosh, M. Shang and T. P. Fehlner, *J. Organomet. Chem.*, **2000**, 614–615, 92–98.
53. R. E. Williams, *Chem. Rev.*, **1992**, 92, 177–207.
54. H. Janet Bullick, P. D. Grebenik, M. L. H Green, A. K. Hughes, C. B. John LeachC and P. C. McGowanb, *J. CHEM. SOC. Dalt. TRANS*, **1995**, 67–75.
55. D. Y. Kim and G. S. Girolami, *J. Am. Chem. Soc.*, **2006**, 128, 10969–10977.
56. A. S. Weller, M. Shang and T. P. Fehlner, *Organometallics*, **1988**, 18, 53–64.
57. D. K. Roy, S. K. Bose, R. S. Anju, V. Ramkumar and S. Ghosh, *Inorg. Chem.*, **2012**, 51, 10715–10722.
58. S. K. Bose, S. Ghosh, B. C. Noll, J.-F. Halet, J.-Y. Saillard and A. Vega, *Organometallics*, **2007**, 26, 5377–5385.
59. A. M. V. Brânzanic, A. Lupan and R. B. King, *Dalt. Trans.*, **2015**, 44, 7355–7363.
60. A. M. V. Brânzanic, A. Lupan and R. B. King, *Organometallics*, **2014**, 33, 6433–6451.
61. S. Aldridge, H. Hashimoto, K. Kawamura, M. Shang and T. P. Fehlner, *Inorg. Chem.*, **1998**, 37, 928–940.
62. A. M. V Brânzanic, A. Lupan and R. B. King, *J. Organomet. Chem.*, **2015**, 792, 74–80.
63. A. M. V. Brânzanic, A. Lupan and R. B. King, *Dalt. Trans.*, **2016**, 45, 9354–9362.
64. R. Borthakur, S. Kar, S. K. Barik, S. Bhattacharya, G. Kundu, B. Varghese and S. Ghosh, *Inorg. Chem.*, **2017**, 56, 1524–1533.
65. B. Mondal, R. Bag and S. Ghosh, *Organometallics*, **2018**, 37, 2419–2428.
66. S. Aldridge, M. Shang and T. P. Fehlner, *J. Am. Chem. SOC*, **1998**, 120, 2586–2598.
67. B. R. Crane, L. M. Siegel and E. D. Getzoff, *Biochemistry*, **1997**, 36, 12120–12137.
68. H. D. Peck, T. Lissolo and J. A. Cole, *Symposium of the Society of General Microbiology – The Nitrogen and Sulfur Cycles*, Cambridge University Press, Cambridge, **1988**.
69. A. Messerschmidt, R. Huber, T. Poulos and K. Wieghardt, *Handbook of Metalloproteins*, Wiley, 2001, John Wiley & Sons Ltd, Chichester, **2001**.
70. T. Akashi, T. Matsumura, T. Ideguchi, K. Iwakiri, T. Kawakatsu, I. Taniguchi and T. Hase, *J. Biol. Chem.*, **1999**, 274, 29399–29405.
71. K. Sekine, M. Fujiwara, M. Nakayama, T. Takao, T. Hase and N. Sato, *FEBS J.*, **2007**, 274, 2054–2069.
72. N. Sato, M. Nakayama and T. Hase, *FEBS Lett.*, **2001**, 487, 347–350.

73. K. Sekine, T. Hase and N. Sato, *J. Biol. Chem.*, **2002**, 277, 24399–24404.
74. G. C. Cannon, L. N. Ward, C. I. Case and S. Heinhorst, *Plant Mol. Biol.*, **1999**, 39, 835–845.
75. B. R. Crane, L. M. Siegel and E. D. Getzoff, *Science*, **1995**, 270, 59–67.
76. L. M. Siegel, D. C. Rueger, M. J. Barber, R. J. Krueger, N. R. Orme-Johnson and W. H. Orme-Johnson, *J. Biol. Chem.*, **1982**, 257, 6348–6350.
77. J. A. Christner, E. Munch, P. A. Janick and L. M. Siegel, *J. Biol. Chem.*, **1981**, 256, 2089–2101.
78. B. R. Crane, L. M. Siegel and E. D. Getzoff, *Biochemistry*, **1997**, 36, 12101–12119.
79. M. Surducan, D. Lup, A. Lupan, S. V. Makarov and R. Silaghi-Dumitrescu, *J. Inorg. Biochem.*, **2013**, 118, 13–20.
80. M. Surducan, A. M. V. Brânzanic and R. Silaghi-Dumitrescu, *Int. J. Quantum Chem.*, **2018**, 118, 2–10.
81. M. Surducan, S. V. Makarov and R. Silaghi-Dumitrescu, *Eur. J. Inorg. Chem.*, **2014**, 34, 5827–5837.
82. R. Silaghi-Dumitrescu and S. V. Makarov, *Int. J. Quantum Chem.*, **2012**, 112, 900–908.
83. E. Sigfridsson, M. H. M. Olsson and U. Ryde, *J. Phys. Chem. B*, **2001**, 105, 5546–5552.
84. E. Sigfridsson, M. H. M. Olsson and U. Ryde, *Inorg. Chem.*, **2001**, 40, 2509–2519.
85. J. Ballmann, A. Albers, S. Demeshko, S. Dechert, E. Bill, E. Bothe, U. Ryde and F. Meyer, *Angew. Chemie - Int. Ed.*, **2008**, 47, 9537–9541.
86. J. Ballmann, S. Dechert, E. Bill, U. Ryde and F. Meyer, *Inorg. Chem.*, **2008**, 47, 1586–1596.
87. M. G. G. Fuchs, F. Meyer and U. Ryde, *J. Biol. Inorg. Chem.*, **2010**, 15, 203–212.
88. M. G. G. Fuchs, S. Dechert, S. Demeshko, U. Ryde and F. Meyer, *Inorg. Chem.*, **2010**, 49, 5853–5858.
89. C. Greco, M. Bruschi, J. Heimdal, P. Fantucci, L. De Gioia and U. Ryde, *Inorg. Chem.*, **2007**, 46, 7256–7258.
90. U. Ryde, C. Greco and L. De Gioia, *J Am Chem Soc*, 132, 4512–4513.
91. M. Bruschi, C. Greco, M. Kaukonen, P. Fantucci, U. Ryde and L. De Gioia, *Angew. Chemie - Int. Ed.*, **2009**, 48, 3503–3506.
92. C. Greco, P. Fantucci, L. De Gioia, R. Suarez-Bertoa, M. Bruschi, J. Talarmin and P. Schollhammer, *Dalt. Trans*, 39, 7320–7329.
93. C. Greco, M. Bruschi, P. Fantucci, U. Ryde and L. Dea Gioia, *Chem. - A Eur. J.*, **2011**, 17, 1954–1965.
94. K. Haufschildt, S. Schmelz, T. M. Kriegler, A. Neumann, J. Streif, H. Arai, D. W. Heinz and G. Layer, *J. Mol. Biol.*, **2014**, 426, 3272–3286.
95. H. L. Schubert, E. Raux, A. A. Brindley, H. K. Leech, K. S. Wilson, C. P. Hill and M. J. Warren, *EMBO J.*, **2002**, 21, 2068–2075.
96. M. E. Stroupe, H. K. Leech, D. S. Daniels, M. J. Warren and E. D. Getzoff, *Nat. Struct. Biol.*, **2003**, 10, 1064–1073.
97. B. Kushkuley and S. S. Stavrov, *Biophys J*, **1997**, 72, 899–912.
98. R. Schnell, T. Sandalova, U. Hellman, Y. Lindqvist and G. Schneider, *J. Biol. Chem.*, **2005**, 280, 27319–27328.
99. S. Nakano, M. Takahashi, A. Sakamoto, H. Morikawa and K. Katayanagi, *Protein Sci.*, **2012**, 21, 383–395.
100. T. F. Oliveira, C. Vornrhein, P. M. Matias, S. S. Venceslau, I. A. C. Pereira and M. Archer,

- J. Biol. Chem.*, **2008**, 283, 34141–34149.
101. M. Jormakka, S. Törnroth, B. Byrne and S. Iwata, *Science (80-)*, **2002**, 295, 1863–1868.
 102. Zhou; Cai; Holm; *Inorg. Chem.*, **1996**, 35, 2767.
 103. L. Cai and R. H. Holm, *J. Am. Chem. Soc.*, **1994**, 116, 7177–7188.
 104. E. N. Mirts, I. D. Petrik, P. Hosseinzadeh, M. J. Nilges and Y. Lu, *Science (80-)*, **2018**, 361, 1098 LP – 1101.
 105. K. Kitaura and K. Morokuma, **1976**, X, 325–340.
 106. K. Morokuma, *J. Chem. Phys.*, **1971**, 55, 1236–1244.
 107. I. Mayer, *Chem. Phys. Lett.*, **1983**, 97, 270–274.
 108. B. a Wittenberg, L. Kampa, J. B. Wittenberg, W. E. Blumberg and J. Peisach, *J. Biol. Chem.*, **1968**, 243, 1854–1862.
 109. B. a Wittenberg, L. Kampa, J. B. Wittenberg, W. E. Blumberg and J. Peisach, *J. Biol. Chem.*, **1968**, 243, 1863–1870.
 110. J. Peisach, W. E. Blumberg, B. A. Wittenberg and J. B. Wittenberg, *J. Biol. Chem.*, **1968**, 243, 1871–1880.
 111. M. D. Clay, C. A. Cosper, F. E. Jenney, M. W. Adams and M. K. Johnson, *Proc. Natl. Acad. Sci. USA*, **2003**, 100, 3796–3801.
 112. P. A. M. Dirac, *R. Soc.*, **1929**, 123, 714-- 733.
 113. J. C. Slater, *Phys. Rev.*, **1951**, 81, 385–390.
 114. P. Hohenberg and W. Kohn, *Phys. Rev.*, **1964**, 136, B864–B871.
 115. L. J. Sham and W. Kohn, *Phys. Rev.*, **1965**, 140, A1133–A1138.
 116. J. P. Perdew and Y. Wang, *Phys. Rev. B*, **1992**, 45, 244–249.
 117. A. D. Becke, *Phys. Rev. A*, **1988**, 38, 3098–3100.
 118. R. Ahlrichs, M. Bär, M. Häser, H. Horn and C. Kölmel, *Chem. Phys. Lett.*, **1989**, 162, 165–169.
 119. J. Tao, J. P. Perdew, V. N. Staroverov and G. E. Scuseria, *Phys. Rev. Lett.*, **2003**, 91, 146401–146404.
 120. S. Grimme, *J. Comput. Chem.*, **2006**, 27, 1787–1799.
 121. A. V. Krukau, G. E. Scuseria, J. P. Perdew and A. Savin, *J. Chem. Phys.*, **2008**, 129, 1–8.
 122. J. P. Perdew, M. Ernzerhof and K. Burke, *J. Chem. Phys.*, **1996**, 105, 9982–9985.
 123. A. D. Becke, *J. Chem. Phys.*, **1993**, 98, 1372–1377.
 124. S. Grimme, *J. Chem. Phys.*, **2006**, 124, 034108.
 125. O. Treutler and R. Ahlrichs, *J. Chem. Phys.*, **1995**, 102, 346–354.
 126. K. Eichkorn, M. Htiser, R. Ahlrichs, K. Eichkorn, O. Treutler, H. Marco and R. Ahlrichs, *Chem. Phys. Lett.*, **1995**, 240, 283–290.
 127. K. Eichkorn, F. Weigend, O. Treutler and R. Ahlrichs, *Theor. Chem. Accounts Theory, Comput. Model. (Theoretica Chim. Acta)*, **1997**, 97, 119–124.
 128. A. Schäfer, H. Horn and R. Ahlrichs, *J. Chem. Phys.*, **1992**, 97, 2571–2577.
 129. S. Grimme, J. Antony, S. Ehrlich and H. Krieg, *J. Chem. Phys.*, **2010**, 132.
 130. A. Schäfer, H. Horn and R. Ahlrichs, *J. Chem. Phys.*, **1994**, 100, 5821–5835.
 131. P. Deglmann, K. May, F. Furche and R. Ahlrichs, *Chem. Phys. Lett.*, **2004**, 384, 103–107.
 132. A. Klamt and G. Schüürmann, *J. Chem. Soc., Perkin Trans. 2*, **1993**, 799–805.
 133. A. Klamt, V. Jonas, T. Bürger and J. C. W. Lohrenz, *J. Phys. Chem. A*, **1998**, 102, 5074–5085.
 134. E. Sigfridsson and U. Ryde, *J. Comput. Chem.*, **1998**, 19, 377–395.
 135. L. Noodleman, *J. Chem. Phys.*, **1981**, 74, 5737.

136. L. Noodleman, T. Lovell, T. Liu, F. Himo and R. A. Torres, *Curr. Opin. Chem. Biol.*, **2002**, 6, 259–273.
137. S. I. Gorelsky, *J. Chem. Theory Comput.*, **2012**, 8, 908–914.
138. T. Lu and F. Chen, *J. Comput. Chem.*, **2012**, 33, 580–592.
139. L. Noodleman, W.-G. Han Du, J. A. Fee, A. W. Götz, R. C. Walker, W.-G. H. Du, J. A. Fee, A. W. Götz and R. C. Walker, *Inorg. Chem.*, **2014**, 53, 6458–6472.
140. P. Su and H. Li, *J. Chem. Phys.*, **2009**, 131.
141. T. Ziegler and A. Rauk, *Theor. Chim. Acta*, **1977**, 46, 1–10.
142. M. Mitoraj and A. Michalak, *J. Mol. Model.*, **2007**, 13, 347–355.
143. M. P. Mitoraj, A. Michalak and T. Ziegler, *J. Chem. Theory Comput.*, **2009**, 5, 962–975.
144. A. Michalak, M. Mitoraj and T. Ziegler, *J. Phys. Chem. A*, **2008**, 112, 1933–1939.
145. P. A. Janick and L. M. Siegel, *Biochemistry*, **1983**, 22, 504–515.
146. H. Nagao, M. Nishino, Y. Shigeta, T. Soda, Y. Kitagawa, T. Onishi, Y. Yoshioka and K. Yamaguchi, *Coord. Chem. Rev.*, **2000**, 198, 265–295.
147. E. Koch, in *Correlated Electrons. From Models to Materials*, eds. E. Pavarini, E. Koch, F. Anders and M. Jarell, Forschungszentrum Jülich GmbH Institute for Advanced Simulation, Jülich, **2012**, p. 31.
148. M. Swart and M. Costas, *Spin States in Biochemistry and Inorganic Chemistry: Influence on Structure and Reactivity*, **2015**.
149. L. Noodleman, D. A. Case, J.-M. Mouesca and B. Lamotte, *J. Biol. Inorg. Chem.*, **1996**, 1, 177–182.
150. L. Pauling, *The Nature of the Chemical Bond*, Cornell University Press, New York, **1960**.
151. R. Dronskowski, *Computational Chemistry of Solid State Materials*, Wiley, Weinheim, **2005**.
152. M. Kaupp, B. Metz and H. Stoll, *Angew. Chem., Int. Ed.*, **2000**, 39, 4607–4609.
153. M. Boggio-Pasqua, A. I. Voronin, P. Halvick and J. C. Rayez, *J. Mol. Struct. THEOCHEM*, **2000**, 531, 159–167.
154. A. Zerr, G. Miehe, G. Serghiou, M. Schwarz, E. Kroke, R. Riedel, H. Fueß, P. Kroll and R. Boehler, *Lett. to Nat.*, **1999**, 400, 340–342.
155. A. Pecchia, G. Penazzi, L. Salvucci and A. Di Carlo, *New J. Phys.*, **2008**, 10.
156. A. Pecchia and A. Di Carlo, *Reports Prog. Phys.*, **2004**, 67, 1497–1561.
157. J. C. Cuevas and E. Scheer, *Molecular Electronics. An Introduction to Theory and Experiment*, World Scientific, Singapore, **2010**.
158. K. Yoshizawa, *Acc. Chem. Res.*, **2012**, 45, 1612–1621.
159. S. Priyadarshy, S. S. Skourtis, S. M. Risser and D. N. Beratan, *J. Chem. Phys.*, **1996**, 104, 9473–9481.
160. A. Nitzan, *J. Phys. Chem. A*, **2001**, 105, 2677–2679.
161. B. Delley, *J. Chem. Phys.*, **1990**, 92, 508–517.
162. 2017 Dassault Systèmes BIOVIA, Materials Studio, 2017, San Diego: Dassault Systèmes.
163. 2017. L.V. Skripnikov, Chemissian Version 4.53, Visualization Computer Program, www.chemissian.com, .
164. F. T. J. C. C. 2004 O.-12. <http://www.rbvi.ucsf.edu/chimer>. . UCSF Chimera--a visualization system for exploratory research and analysis. Pettersen EF, Goddard TD, Huang CC, Couch GS, Greenblatt DM, Meng EC, .
165. L. Noodleman and D. A. Case, *Adv. Inorg. Chem.*, **1992**, 38, 423.
166. J. P. Launay and M. Verdaguer, *Electrons in Molecules*, Oxford University Press, Oxford,

- revised ed., **2018**.
167. J. J. Warren, M. E. Ener, A. Vlček, J. R. Winkler and H. B. Gray, *Coord. Chem. Rev.*, **2012**, 256, 2478–2487.
 168. J. Geng, K. Dornevil, V. L. Davidson and A. Liu, *Proc. Natl. Acad. Sci.*, **2013**, 110, 9639–9644.
 169. N. A. Tarboush, L. M. R. Jensen, E. T. Yukl, J. Geng, A. Liu, C. M. Wilmot and V. L. Davidson, *Proc. Natl. Acad. Sci.*, **2011**, 108, 16956–16961.
 170. P. L. Dutton, C. C. Page, C. C. Moser and X. Chen, *Nature*, **1999**, 402, 47–52.
 171. C. C. Moser, S. E. Chobot, C. C. Page and P. L. Dutton, *Biochim. Biophys. Acta - Bioenerg.*, **2008**, 1777, 1032–1037.
 172. R. Pietri, E. Román-Morales and J. López-Garriga, *Antioxid. Redox Signal.*, **2010**, 15, 393–404.
 173. B. B. Ríos-González, E. M. Román-Morales, R. Pietri and J. López-Garriga, *J. Inorg. Biochem.*, **2014**, 133, 78–86.
 174. H. D. Arbelo-Lopez, N. A. Simakov, J. C. Smith, J. Lopez-Garriga and T. Wymore, *J. Phys. Chem. B*, **2016**, 120, 7319–7331.
 175. J. A. Berzofsky, J. Peisach and J. A. Alben, *J. Biol. Chem.*, **1972**, 247, 3774–3782.
 176. P. R. O. de Montellano, *Curr. Opin. Chem. Biol.*, **2000**, 221–227.
 177. A. M. V Brânzanic, U. Ryde and R. Silaghi-dumitrescu, *J. Inorg. Biochem.*, **2020**, 203, 110928.
 178. R. Silaghi-Dumitrescu, *Stud. Univ. Babeş-Bolyai, Chem.*, **2007**, 52, 127–130.
 179. R. Silaghi-Dumitrescu, *J. Biol. Inorg. Chem.*, **2004**, 9, 471–476.
 180. A. M. V. Brânzanic, U. Ryde and R. Silaghi-Dumitrescu, *Chem. Commun.*, **2019**, 55, 14047–14049.
 181. D. A. Bryant, C. N. Hunter and M. J. Warren, *J. Biol. Chem.*, **2020**, 295, 6888–6925.
 182. G. Frenking and A. Krapp, *J. Comput. Chem.*, **2007**, 28, 15–24.